THE UNIVERSITY OF MANITOBA

MICROWAVE DOPPLER - EFFECT FLOW MONITOR

by

ABDUL HAMID

A THESIS

SUBMITTED TO THE FACULTY OF GRADUATE STUDIES
IN PARTIAL FULFILLMENT OF THE REQUIREMENTS FOR THE DEGREE
OF MASTER OF SCIENCE

DEPARTMENT OF AGRICULTURAL ENGINEERING

WINNIPEG, MANITOBA

February 1975

MICROWAVE DOPPLER-EFFECT FLOW MONITOR

by

ABDUL HAMID

A dissertation submitted to the Faculty of Graduate Studies of the University of Manitoba in partial fulfillment of the requirements of the degree of

MASTER OF SCIENCE

ABSTRACT

This research was conducted to study the feasibility of using Microwave Doppler radar as a flow monitor for particulate solids. Investigations were performed both with single scattering particles and bulk flows of materials in order to evaluate quantitatively the capabilities and limitations of the Microwave Doppler-Effect Flowmonitor (MDEF). A commercially available X-band Doppler transceiver, operating at a frequency of 10.525 GHz, was used throughout the experiments.

Two basic configurations were considered. In the first configuration, a scattered Doppler signal was obtained from a column of substance passing through a section of rectangular waveguide. The second configuration, involved a Doppler signal from the materials flowing in a dielectric tube located in the field of a horn antenna. Both the monostatic and bistatic configurations were studied.

The relationship between the velocity and the Doppler frequency was verified experimentally for single scattering particles. The relationship between the bulk velocity and the Doppler frequency was derived and verified experimentally for continuous flow of wheat and rapeseeds. The effects of different viewing angles and distances between the antenna aperture and flow field were investigated.

It was concluded that the Doppler radar can be used to measure the average bulk velocity of particulate solids flowing in pipes. When the bulk density and the cross-section area of the pipe are known, the MDEF provides contactless means of monitoring mass flow rate of particulate solids.

ACKNOWLEDGEMENTS

I wish to acknowledge the supervision of Dr. S.S. Stuchly as my advisor and major professor. I am greatly indebted to him for his patient guidance, friendly attitude and constant encouragement throughout the conduct of this project. My sincere thanks are due to Dr. M.A. Rzepecka for her valuable help and deep interest in the project. Her guidance during the period of Dr. Stuchly's absence is gratefully acknowledged.

Acknowledgements are due to Dr. M.A.K. Hamid and Dr. J.S. Townsend for reviewing the manuscript as committee members.

Special thanks go to Mr. W.S. Matulewicz who designed and built an analog frequency meter. The valuable suggestions from him and from Mr. M.T. Faber in problems concerning electronic instrumentation are sincerely acknowledged. The assistance of Messrs. J.G. Putnam, A.E. Krentz and R.H. Mogan in the preparation of the mechanical set-up for the experiments is highly appreciated.

Sincere appreciation is expressed to Miss J. Gourlay for her careful typing of the manuscript.

TABLE OF CONTENTS

LIST OF FIGURES

LIST OF TABLES

LIST OF SYMBOLS

A - Cross-sectional area of the flow field

A_e - Effective antenna aperture

A_r - Effective aperture of the receiving antenna

A_t - Effective aperture of the transmitting antenna

A_1 - Cross-sectional area of the flow control disk

D - Bulk density

E - Maximum amplitude

$|E_i|$ - Magnitude of the incident electric field

$|E_s|$ - Magnitude of the scattered electric field

E_o - Maximum amplitude corresponding to a reference sphere

F - Shape factor

F_o - Noise figure

G - Antenna gain

$|H_i|$ - Magnitude of the incident magnetic field

$|H_s|$ - Magntiude of the scattered magnetic field

K - Proportionality factor between the flow rate and average Doppler frequency

K_1 - Constant depending upon the mixer's induced bias current and applied DC bias

K_2 - Constant which includes the parameters involved in the radar equation

L - Elongation factor

N - number of observations

NP - Noise power

P - Maximum power received

P_o - Maximum power received corresponding to a calibrating sphere

P_r - Power received

P_t - Power transmitted

Q - Mass flow rate

$\bar{Q}$ - Average mass flow rate

R - Radar range

R_o - Distance of free space propagation

R_r - Distance between the receiver and target

R_t - Distance between the transmitter and target

S/N - Signal-to-noise ratio

T - Integration time

V - Volume of the target

V_1, V_2 - Voltages

V_r - Resultant voltage

W - The width of the antenna aperture which controls the radiation pattern in the plane of interest.

a - Correction factor

c - Velocity of propagation of electromagnetic waves

c' - A factor defining the third axis of a spheroid

d - Diameter of the column of a dielectric material

f_o - Frequency of transmission

f_1 - The lowest Doppler frequency of interest

f_2 - The highest Doppler frequency of interest

f_d - Doppler frequency

$\bar{f}_d$ - Mean Doppler frequency

$f_{d_{av}}$ - Long time average Doppler frequency in continuous flow

$f_{d_{\theta r}}$ - Doppler frequency corresponding to angle θ_r of the receiver

$f_{d_{45}}$ - Doppler frequency corresponding to the viewing angles of 45° for both the transmitter and receiver.

g - Acceleration due to gravity

k - $\lambda g/\lambda$

k' - $2\pi/\lambda$

$s_{f_{av}}$ - Standard deviation of the average Doppler frequency

s_{f_i} - Standard deviation of the instantaneous Doppler frequency

t - Time

u - Initial velocity

v - Velocity of the target in free space

$\bar{v}$ - Average bulk velocity

v_a - Velocity measured from the photoresistor pulses

v_g - Velocity of the target in the waveguide configuration

v_i - Instantaneous velocity

v_m - Maximum theoretical velocity

v_r - Velocity in the direction of radar

y - Vertical distance between the initial and final velocity measuring points

Δf_d - Bandwidth of the Doppler frequency spectrum

Δv - Error in the velocity measurement

$\Delta\theta$ - Antenna beamwidth

δf - Error in the frequency measurement

$\delta\theta$ - Error in measurement of the viewing angle

ε'_r - Relative dielectric constant

θ - Viewing angle

θ_g - Angle of intersection between the waveguide section and the circular tube

θ_h - Viewing angle of the upper-most antenna ray

θ_i - Instantaneous viewing angle

θ_{id} - Angle of incidence

θ_{id} - Angle of incidence

θ_{ℓ} - Viewing angle of the lower-most antenna ray

θ_o - Axial viewing angle

θ_r - Viewing angle of the receiver

θ_{rf} - Angle of refraction

θ_t - Viewing angle of the transmitter

λ - Free space wavelength

λ_d - Wavelength in the dielectric medium

λ_g - Wavelength in the waveguide

μ_r - Relative permeability

σ - Backscattering radar cross-section in the free space configuration

σ_o - Backscattering cross-section of a calibrating sphere

σ_b - Bistatic radar cross-section

σ_g - Radar cross-section in the waveguide configuration

σ_{g_o} - Radar cross-section of a calibrating sphere in the waveguide configuration

σ_o - Radar cross-section of a calibrating sphere in the free space configuration

ϕ_1, ϕ_2 - Phase difference

ω_d - Angular Doppler frequency

CHAPTER 1

INTRODUCTION

There are many well-known methods of measuring flow rate such as obstruction meters, drag effect meters, electromagnetic flow meters and turbine meters (Considine and Rose, 1964). All these methods, although successfully used for gas and liquid flows, can not be adapted to the flow metering of viscoelastic fluids, particulate solids and slurries, since the sensor usually obstructs the flow and causes blockages. Monitoring the flow fields of particulate solids, whether created by conveyor belt, pneumatic or hydraulic transport or due to free fall as from a hopper, has been one of the more experimentally difficult problems in flow measurements. A number of solutions have been proposed to overcome these difficulties including an obscure technique of measuring capacitance or resistance "noise" in the flow field (Lazenby and Davies, 1973) and culminating in the microwave Doppler flowmeter technique.

Microwave Doppler radar has been used for many years in navigation and traffic control. Its capabilities and limitations in these applications have been studied in great detail (Barlow, 1949; Skolnik, 1962). Its application as a flow monitor, which has been suggested only recently (Ellerbruch, 1970; Harris, 1970; Parker, 1970), shows the considerable promise for the solution of important flow measurement problems in the chemical and food processing industries.

There are several valuable features of the Doppler radar flowmeter. The measurements are contactless and the meter does neither obstruct the flow nor disturb the monitored process. Being remote in principle, it is particularly applicable to hostile environments and inaccessible situations. The response of the system is fast and data

processing is easy which makes the instrument very suitable for automatic control systems.

An optical equivalent of the MDEF [Microwave Doppler-Effect Flow Monitor], the laser anemometer, has already been developed to a very high degree of sophistication; and has been described and analysed in numerous papers and technical reports (DISA, 1973). The laser Doppler meter, it is claimed (Harris, 1970), can read the speed and length of continuous paper, plastic, metal or textile strip - any suitable reflector of light in fact. Although the MDEF does not possess the potentials of its optical equivalent, particularly in measurement of local velocities as well as in spatial resolution and uncertainty of measurements, it can be used successfully for monitoring non-transparent substances, where the laser anemometer fails.

It was the purpose of this research to study the feasibility of the utilization of the microwave Doppler radar for monitoring of the flow rate of particulate solids. The specific objective included the development of the relationship between the Doppler frequency and the bulk velocity of grains moving in pipes. The flow rate was assumed to be proportional to the bulk velocity of the material. The determination of the cross-sectional area of the flow field and the material density are separate problems and were not dealt with in this research.

CHAPTER 2

REVIEW OF LITERATURE

The field of flowmetering is as old as the recorded history and has been ever expanding. A survey made a few years ago (Cotton, 1966) showed that over several decades prior to 1900, more patents were issued for inventions relating to flowmetering than any other comparable single field of engineering.

Many novel instruments are available for monitoring the flow rate of fluids (Bean, 1966). Steam at the temperature of 600°C and pressure of 136 atm may be metered with a flow nozzle, while liquid sodium can be measured with a magnetic flowmeter. A displacement type meter can be used to measure the flow rate of liquid methane, hydrogen or helium. A magnetic flowmeter, 1.8 m in diameter, measures the volumetric flow rate in a sewage system up to 11.5 m^3/s, while an orifice meter in a 0.9mm pipe line tallies up to 2×10^6 m^3 of fuel gas per day. In a laboratory, a reagent flowing the equivalent of a drop per minute can be monitored with a bubblemeter. Turbine meters are being applied to many fluid metering situations for gases as well as liquids. Recently, the laser anemometers have become available for measurements of local velocities in the turbulent flow fields.

The basic principles used for monitoring the flow rate of fluids apply equally well to granular materials. However, difficulties of conveying the material through the meter drastically limit practical application of the modified forms of these meters. Several devices have been suggested for detection and measurement of the flow rate of particulate solids; but due to variety of materials handled and conveying systems employed, none has achieved the wide-spread popularity as a versatile

and non-contact industrial device.

By far, continuous weighing is the most common method of measuring the flow rate of particulate solids. The material passing a fixed point can be weighed, or the decrease in weight of a hopper can be measured (Beck and Wainwright, 1969). Early methods of weighing on a conveyor belt (Kirwan and Demler, 1955) required part of the belt to be supported from a pivoted arm. The weighing mechanism restored the belt to the equilibrium position; the restoring force being proportional to the weight of the material on the belt. Modern methods of continuous weighing employ load cells to measure the weight of material and a tachometer for measuring the speed of the belt (Gravan, 1964). Continuous weighing is basically an accurate method of measuring solid flow rates on a conveyor belt, but it is not suitable for pneumatic conveyors. Furthermore, the instruments require a fair amount of maintenance which increases the cost of operation.

The pressure drop technique of flow measurement in pneumatic conveyors has been known for a number of years (Carlson et al., 1948; Farbar, 1952). The technique has not been widely accepted in industrial plants because the instrument introduces an obstruction in the pipe carrying the test material, thus, causing blockages.

Different methods, relying on the principle of vibrations produced in a probe, have been used to detect the flow failures of granular or powdered solids (Beck and Wainwright, 1969). The flowing material causes the probe to vibrate which indicates that the material is flowing. When the material ceases to flow, the level of vibrations falls and flow failure can be indicated by a suitable alarm system. Vibration methods, although suitable for very dense - phase flow systems, are un-

suitable for light-phase pneumatic conveyors. The probe has to be inserted into the conveyor system and this normally causes blockages.

A spiral vane flowmeter, for measuring the volumetric flow rate of granular solids flowing through vertical ducts, has been reported by Brown et al. (1962). The movement of granular solids in the duct causes the vane to rotate and the number of revolutions of the vane is a measure of the volumetric flow rate. The spiral vane meter can be used only in vertical ducts of diameters larger than 0.4 m The meter will not measure the flow rate of pneumatically conveyed material, because the rate at which the vane turns is influenced by the air velocity. It has moving parts which require considerable maintenance and it tends to restrict the flow.

A few scattered efforts have been made in the past to employ the principle of change of momentum to measure flow rates of particulate solids. Patents were granted (Bousser, 1904; Merchen, 1929) for mechanisms working on this principle to regulate the flow of grain. An inclined plate device working on this principle was suggested by Dean (1955). In this device, the granular material is allowed to fall onto an inclined plate attached to a rigid beam. The beam is pivoted about a point near its center, and moment is measured by a force balance unit. If the velocity of the material is constant, the force on the plate is proportional to the mass flow rate of the material. This device can only be used with dense flowing solids that are falling freely under gravity. The meter is a potential source of obstruction in the system and its calibration depends upon the position where the material falls onto the plate. The mass flowmeter reported by Nolte (1969), senses the change in momentum of the material with an impulse sensor after the material has

fallen a definite distance inside the meter. The motion of the sensor is vertical only. Therefore, the direction of entry of the material has no influence on the calibration of the instrument. Even this meter causes blockages in the conveying system and can not be successfully adapted for pneumatic conveyors. [illegible] the same

Rotating impeller type meters are based on the change of the angular momentum of the measured material. The torque in the supporting shaft, produced due to change in angular momentum, is proportional to the mass flow rate. A mass flowmeter working on this principle has been developed by the Wallace and Tiernan, Inc. (Kirwan and Demler, 1955). The same principle is utilized in another practical flowmeter reported by Henderson (1966). In that instrument, the impeller consists of 8 vertical vanes and the torque is measured with 4 strain gauges. The strain gauges are positioned in such a way that they measure only the torque and are not influenced by the bending moment (bending moment is produced by solids not being uniformly distributed about the central axis of the shaft). The rotating impeller method of flow measurement is not suitable for pneumatic conveyors, since the material must fall freely under gravity onto the impeller. The meter has rotating parts which require considerable maintenance and the instrument tends to cause blockages in the conveying system.

The Optical methods can be used to detect or measure the volumetric flow rate of powders (Beck and Wainwright, 1969). These methods are generally unreliable in situations where the optical surface can become dirty, and are applicable only to the materials having a high coefficient of reflection.

The nucleonic absorption technique for measuring the mass flow rate of granular solids on conveyor belts has been reported by Perkovski (1963) and Rowe (1963). The method is based on the fact that the amount of gamma radiation absorbed depends upon the mass of the material in the path of the radiation. The relationship between the absorption and mass flow rate is claimed to be linear over a limited flow range. Variations in the moisture content and density introduce errors. This is a non-contact method of measuring the loading of the material. It can be used in pneumatic conveyors, only, if the velocity is measured independently.

Beck et al., (1968) reported a method of measuring powder flow in a pneumatic conveyor using a capacitance transducer. The velocity was determined by measuring the transit time of the flow pattern between the two fixed points in the conveyor. The method utilized complex mathematical calculations, necessitating an on-line computer.

A radio active tracer technique for measuring the corn kernel velocities in pneumatic conveyors was used by Keller et al., (1971). The path of the particle treated with a radioactive substance can be traced in the conveying line without alteration of the conveyor system. The bulk velocity of a material can not be estimated accurately from the velocity of a single particle, and, of course, the contamination of many grains can not be allowed due to health hazards.

The latest developments in the flow metering of particulate solids utilize the phenomenon of capacitance "noise". This phenomenon was first identified in Fielden's research department and later termed as "Worland effect". Granular materials and powders moving in a pipe produce rapid fluctuations in capacitance. Beck (1968) of Bradford University developed the relationship between the capacitance noise and the mass flow in

pneumatic conveying systems. He concluded that the material in pipes moves in 'bunches'. This causes capacitance variations proportional to the mass flow of the material.

The Flowmeters, based on the principle of capacitance 'noise', have been described by Powley (1972) and Lazenby et al. (1973). These meters do not give an accurate mass flow rate in the situations where the velocity of the conveyed material is not constant. The meters give, in fact, the loading factor, which may give a true mass flow rate if multiplied by the actual velocity. The technique of cross-correlation, the same as used by Beck et al. (1968), was suggested (Lazenby et al. 1973) for measuring the velocity.

The microwave Doppler flowmeter technique was suggested by Ellerbruch (1970) and Parker (1970). Some of the qualitative studies to apply this technique to the flow metering of particulate solids were made by Harris (1970). Hannir (1970) suggested the use of the Doppler radar for the detection of flow failures in granular or powder flow. The Doppler radar system seems to be a promising device for contactless measurements of flow rate of particulate solids.

CHAPTER 3

THEORETICAL CONSIDERATIONS

3.1 Principle of Operation of MDEF

The MDEF utilizes the principle of continuous wave (CW) Doppler radar. In the CW Doppler radar, the transmitter sends out continuous electromagnetic signals and the receiver also continuously listens to return signals. The return signal carries information about the target approach velocity due to the Doppler effect. The Doppler principle implies that if either the source of oscillation or observer of oscillation is in motion, an apparent shift in frequency results. The difference between the frequency of the transmitted and reflected signals is referred to as the Doppler frequency, which is directly proportional to the target approach velocity. The relationship between the velocity and the Doppler frequency can be formulated as follows (Skolnik, 1962):

$$f_d = \frac{2f_o}{c} v \cos\theta \qquad (3.1)$$

and hence

$$v = \frac{c}{2f_o} f_d/\cos\theta \qquad (3.2)$$

where, f_d is the Doppler frequency in Hz, f_o is the frequency of transmission in Hz, c is the velocity of propagation of the electromagnetic waves in m/s, and θ is the viewing angle, i.e., the angle between the electrical axis of the antenna and the velocity vector, in degrees.

For example, at the viewing angle equal to zero, and the frequency of transmission equal to 10.525 GHz, the velocity of one m/s is equivalent to the Doppler frequency of 70.07 Hz.

The volumetric flow rate of a test material flowing through a

given area A is proportional to the velocity. When the bulk density of the material is also known, the velocity measured by the Doppler radar is a measure of the mass flow rate, Q. Thus,

$$Q = ADv \tag{3.3}$$

When A is in m^2, D in kg/m^3 and v in m/s, Q is then in kg/s.

3.2 Practical Microwave Doppler Radar

Fig. 3.1 shows a typical block diagram of a monostatic Doppler radar. The transmitter generates a continuous wave at a frequency f_o. An antenna beams the transmitted waves towards the moving target. A portion of the radiated energy is scattered by the target in the direction of the radar where it is collected by the antenna. The received signal is shifted in frequency in respect to the transmitted frequency f_o by $\pm f_d$, depending upon the velocity of the target. The plus sign applies to an approaching target, while the minus sign refers to a receding target. In the monostatic radar, a single antenna serves the purpose of both the transmission and reception of the signals. The need for separate antennas is eliminated by a ferrite circulator. The circulator isolates the outgoing and incoming signals from each other, even though they pass in and out through a common port. In practice, it is not possible to eliminate completely the transmitter leakage. However, a moderate amount of power, entering the receiver along with the echo signal, provides the local oscillator signal necessary for the detection of the Doppler frequency shift. The received echo signal at a frequency $f_o \pm f_d$ is heterodyned in the mixer with the reference signal, at a frequency f_o, to produce a Doppler signal at a frequency f_d. The sign of f_d is lost in this process. The output of the mixer is fed to an

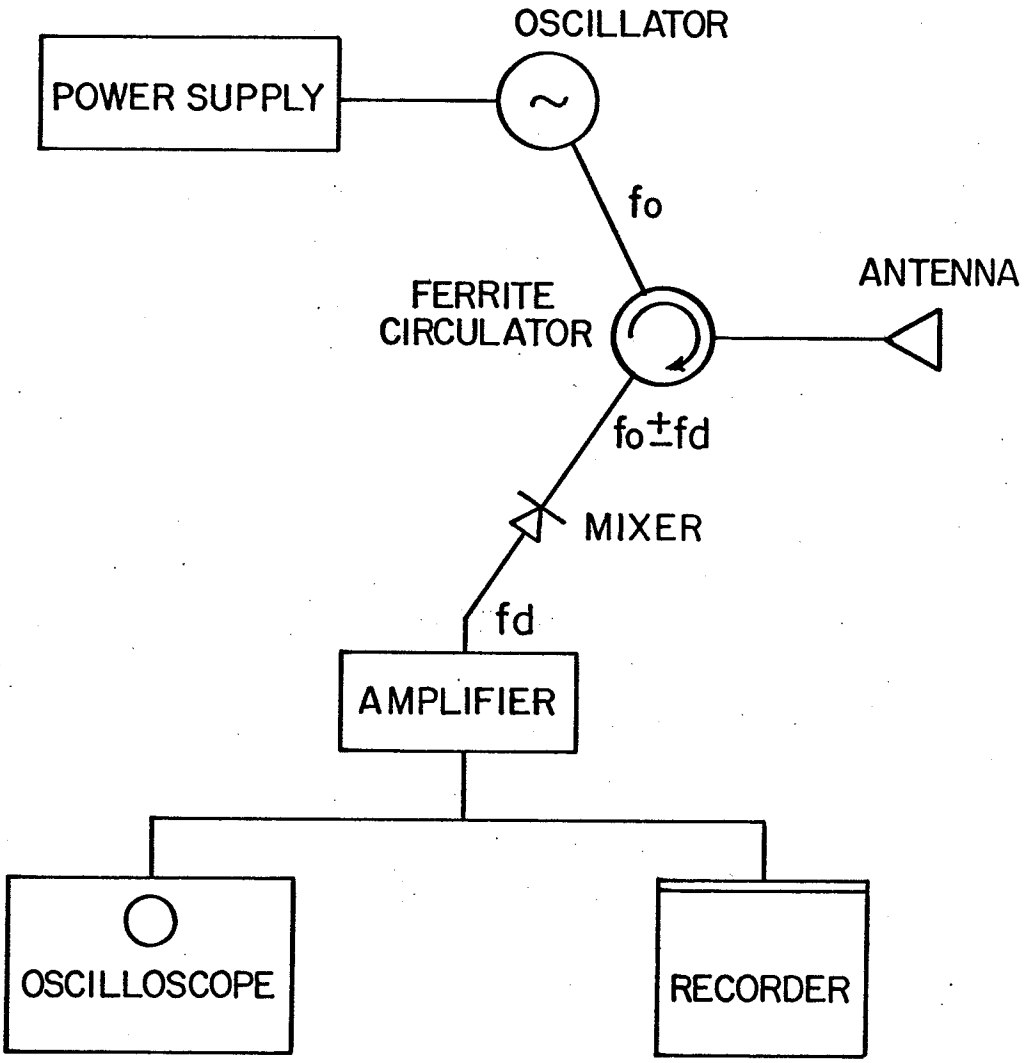

Fig. 3.1 Block Diagram of a Typical Doppler Radar

amplifier to boost the signal to the level convenient for processing. The specific nature of the signal processing and indicating units will, of course, depend upon the task for which the Doppler radar system is being used. An oscilloscope and a recorder were used, throughout this study, to display and record the signals.

3.3 Modes of operation

Two basic modes of operation of the MDEF are possible: the free space transmission and backscattering, and waveguide transmission and reflection mode. Furthermore, two configurations are possible in the free space mode: the monostatic and bistatic.

3.3.1 Free Space Mode

In the free space mode, the antenna illuminates a section of a pipe transparent to microwaves. The pipe should be non-metallic or, otherwise, the signal may be obtained by providing a plastic, fiber glass, quartz or lead free glass window in the metal pipe (Harris, 1970). *Monostatic Configuration:* A simplified diagram of the system using the monostatic configuration is shown in Fig. 3.2. This configuration utilizes a single antenna for transmission and reception of the microwave signals. The isolation between the two signals is provided by a ferrite circulator. In modern Doppler transceivers, the transmitter and receiver are integrated in one unit. Since only one antenna is needed, this configuration has an obvious advantage of lower cost when compared with the bistatic configuration. The relation between the velocity and the Doppler frequency in this configuration is relatively simple and the information about the target can be extracted relatively easily. Another advantage of the monostatic configuration is that only one mounting is required, as compared to two mountings required in the

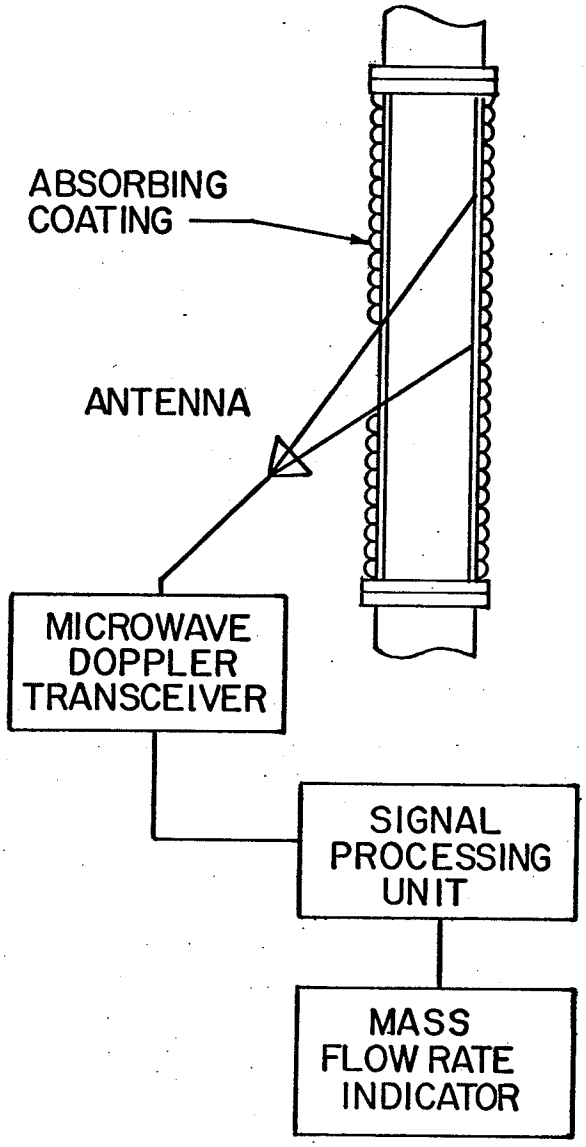

Fig. 3.2 MDEF in the Monostatic Configuration

bistatic configuration. The equations for the velocity and flow rate in the monostatic configuration are discussed in section 3.1.

Bistatic Configuration: In the bistatic configuration, the transmitter and receiver are at different locations and two separate antennas are used for transmitting and receiving of the signals. CW radar requires considerable isolation between the transmitter and receiver in order to prevent the transmitted signal from leaking into the receiver. The isolation is readily obtained in the bistatic radar because of the inherent separation between the transmitter and receiver. The utilization of two antennas increases the cost of the radar. Although the use of two antennas can provide a high degree of isolation, loss of effective aperture is a consequence. A single antenna of total area 2A provides a 6 dB higher sensitivity than two separate antennas each of the area A (Skolnik, 1962). Furthermore, two separate antennas usually result in a more difficult mechanical mounting. Nevertheless, the application of the bistatic system in flow measurement has the advantage of better definition of the measuring area, because the measured volume is determined by the overlapping beams of the transmitting and receiving antennas.

If the angle between the transmitter and receiver is different from 180°, Eq. (3.2) can be applied to the bistatic configuration as follows:

$$v = \frac{c}{2f_o} \cdot f_d/(\cos\theta_t + \cos\theta_r)$$

and

$$Q = AD \frac{c}{f_o} \cdot f_d/(\cos\theta_t + \cos\theta_r) \qquad (3.4)$$

where Q is the flow rate in kg/s, θ_t is the viewing angle of the trans-

mitter in degrees, θ_r is the viewing angle of the receiver in degrees, A is the area of flow in m^2, and D is the bulk density in kg/m^3. Other symbols are the same as in Eq. (3.2).

A simplified diagram of the MDEF utilizing the bistatic configuration is shown in Fig. 3.3.

3.3.2 Waveguide mode

A diagram of the Doppler flow monitor, utilizing a waveguide sensor, is shown in Fig. 3.4. A section of a standard rectangular waveguide intersects with a dielectric pipe carrying the material at a certain angle usually less than 45°. The metal tube surrounding the dielectric pipe, crossing the rectangular waveguide, forms a circular waveguide operating below cut-off. The interaction between the flowing material and the electromagnetic wave is confined to the section of the dielectric pipe inside the rectangular waveguide. Only the monostatic configuration of the flowmeter is possible in this mode. The microwave transceiver is connected to one end of the waveguide section, while the other end is terminated by a matched load.

The waveguide mode has several essential advantages when compared with the free space mode. It is much more sensitive (Eq. 3.8), so that very small nonuniformities can be detected. It is free from interfering effects and secondary reflections from the surrounding objects. Further advantages include the compactness and simplicity of the sensor.

The major limitation of this arrangement comes from the fact that for an X-band sensor, the diameteroof dielectric pipe carrying the material, can not be larger than 0.008 m for most practical materials.

The relationship between the velocity and the Doppler frequency in the waveguide mode can be obtained by substituting λg instead of λ:

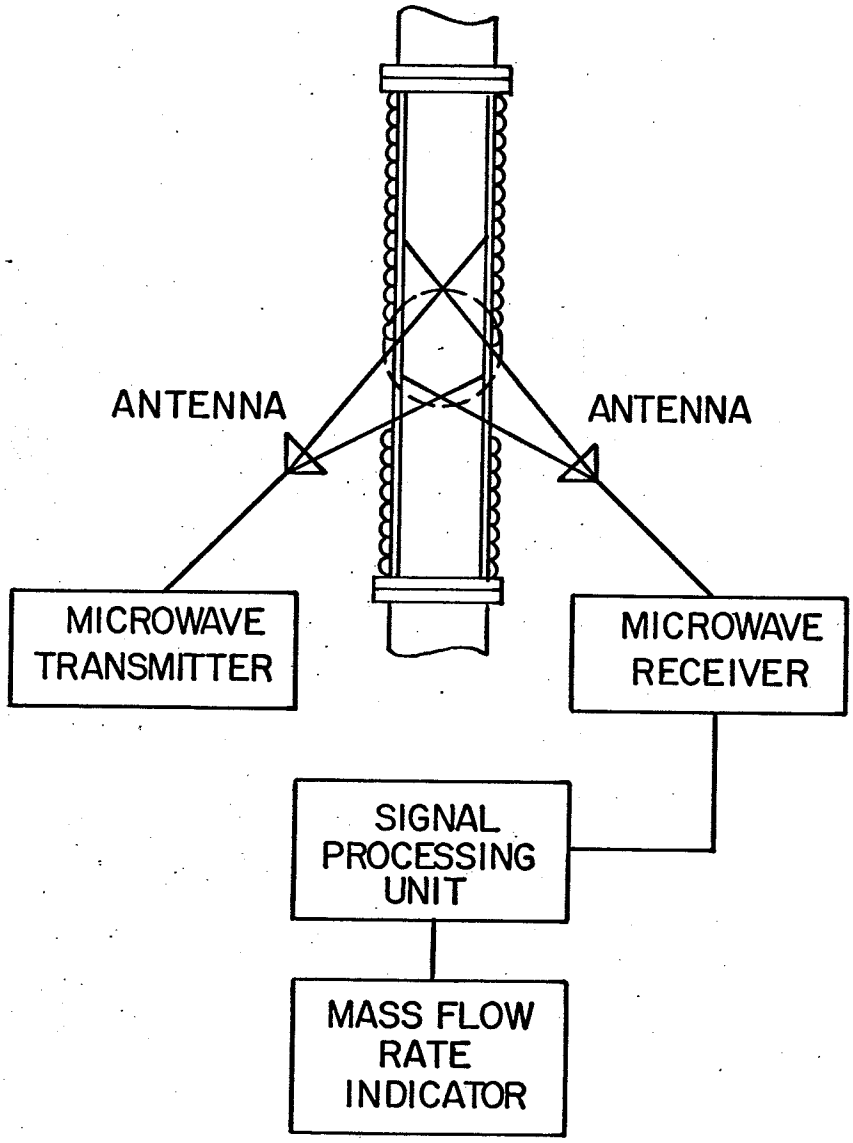

Fig. 3.3 MDEF in the Bistatic Configuration

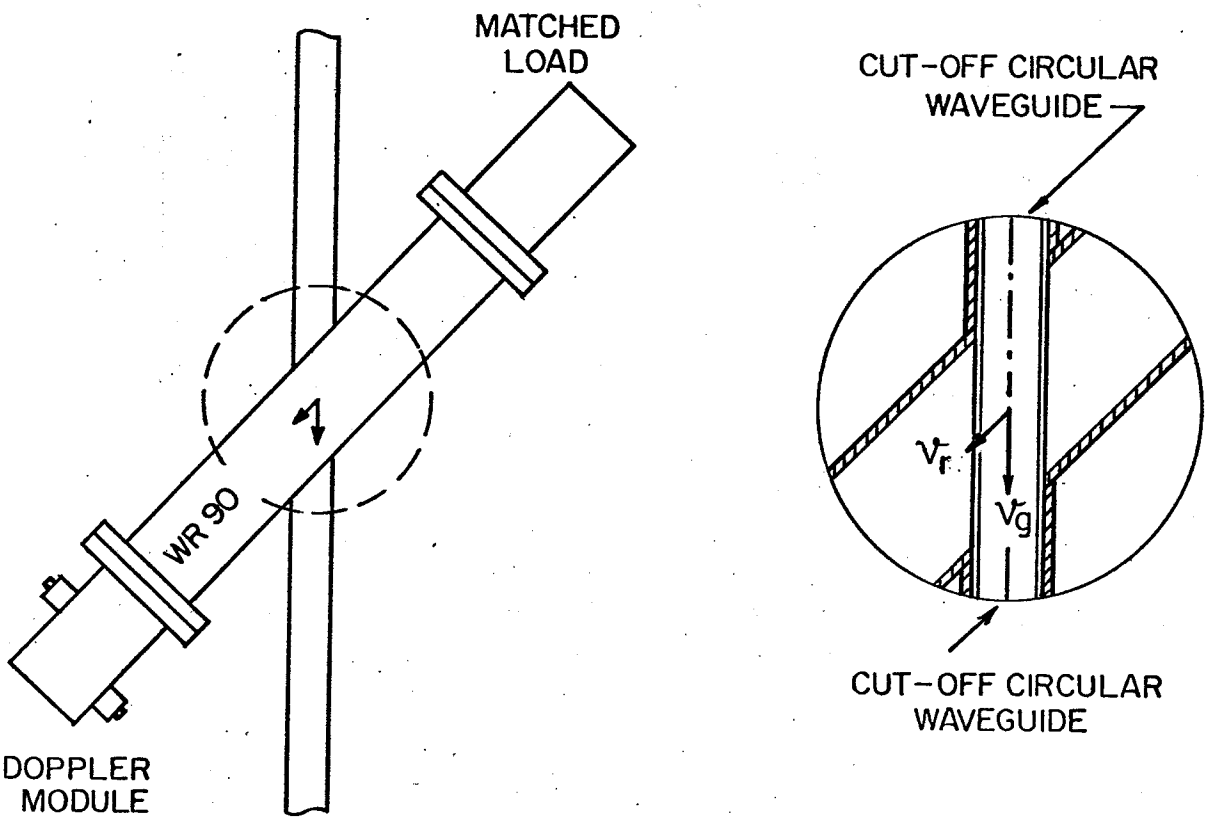

Fig. 3.4 MDEF in the Waveguide Mode

$$v_g = k \frac{c}{2f_o} f_d/\cos\theta_g \qquad (3.5)$$

where $k = \lambda g/\lambda$, λg is the waveguide wavelength in m, λ is the free space wavelength in m, v_g is the velocity of the target in m/s and θ_g is the angle of intersection of the waveguide with the pipe. Other symbols have the same meaning as in Eq. (3.2) and Eq. (3.3).

3.4 Radar Equation

The basic radar equation in the monostatic configuration can be stated as follows (Skolnik, 1962):

$$P_r = \frac{P_t A_e^2 \sigma}{4\pi \lambda^2 R^4} \qquad (3.6)$$

where, $A_e = \frac{G\lambda^2}{4\pi}$, A_e is the effective antenna aperture in m^2, P_r is the maximum theoretical received power in W, P_t is the transmitted power in W, σ is the radar cross-section in m^2, R is the radar range in m, G is the antenna gain, and λ is the free space wavelength in m.

This simplified version of the radar equation does not adequately predict the power received. In practice, the power received may be much smaller than that given by Eq. (3.5). There are many losses which can occur throughout the system. Another important factor is the statistical nature of some parameters, such as radar cross-section. The equation does,however, indicate that the received power, for a given radar cross-section, can be increased by increasing the transmitted power, by decreasing the range, and by utilizing an antenna of large aperture.

Noise is one of the main factors limiting the radar performance. The major factors contributing to the radar noise are: the surrounding moving or stationary objects, the stray reflections, and the noise generated inside the system.

The receiver noise power is a function of the noise generated by the Gunn diode and the conversion loss of the mixer. A simplified but adequate expression for the total noise power (refered to the RF port) of the Doppler receiver, is given by (HP. application note, 1971)

$$NP = 10 \log \left[K_1 \ln \frac{f_2}{f_1}\right] \tag{3.7}$$

where NP is the noise power in dBm, f_1 is the lowest Doppler frequency of interest in Hz, f_2 is the highest Doppler frequency of interest in Hz, and K_1 is a constant whose value depends upon the total detector current (HP application note, 1971).

Eq. (3.7) indicates that the noise power can be decreased by limiting the bandwidth of the receiver.

The radar equation [Eq. (3.6)] can be extended to the bistatic radar as follows (Skolnik, 1962):

$$P_r = \frac{P_t A_t A_r \sigma_b}{4\pi \lambda^2 R_t^2 R_r^2} \tag{3.8}$$

where P_r is the maximum received power in W, P_t is the transmitted power in W, A_t is the effective aperture of the transmitting antenna in m^2, A_r is the effective aperture of the receiving antenna in m^2, R_t is the transmitter-to-target distance in m, R_r is the receiver-to-target distance in m, σ_b is the bistatic radar cross-section in m^2, and λ is the free space wavelength in m.

There are no free space losses in the waveguide configuration. Assuming the losses in the waveguide to be negligible, the radar equation for the waveguide configuration is:

$$P_r = P_f \sigma_g \tag{3.9}$$

where P_r is the power received in W, P_i is the intensity of the incident power in W/m^2, and σ_c is radar cross-section in m^2.

3.5 Radar Cross-Section

The radar cross-section of the scattering object may be defined as follows (Crispin and Siegel, 1968):

$$\sigma = R \longrightarrow \infty \quad 4\pi R^2 \left| \frac{H_s}{H_i} \right|^2$$

$$= R \longrightarrow \infty \quad 4\pi R^2 \left| \frac{E_s}{E_i} \right|^2$$

where R is the distance from the point of observation to the origin of a coordinate system, $|E_i|$ and $|H_i|$ are the magnitudes of the incident electric and magnetic fields, respectively, and $|E_s|$ and $|H_s|$ are the magnitudes of the scattered electric and magnetic fields, respectively.

The radar cross-section may be described as the area intercepting that amount of power which, when scattered equally in all directions, produces an echo at the radar equal to that from the target (Skolnik, 1962). In the monostatic radar, backscattering cross-section is of primary interest, while in the bistatic radar, forward scattering is most important.

Theoretically, the radar cross-section can be determined by solving Maxwell's equations with proper boundary conditions, but this analytical method is applicable to geometrically simple shapes only. The most popular experimental method of determining the radar cross-section of an object is by comparison with a calibrating metal sphere.

The RCS is frequency dependent. Let d denote some characteristic dimension of the scattering object, and L the wavelength of the incident wave, then the region where $d/\lambda \ll 1$, that is, the size of the

object is small compared with the wavelength, is known as the Rayleigh region. On the other extreme is the geometrical optics region, where the wavelength is very small when compared to the dimension of the scattering object, that is $d/\lambda >> 1$. Between the two regions, there is the Mie or resonance region, where the RCS varies oscillatorily with frequency. The RCS of most of the particulate solids of interest falls in the Rayleigh region and, therefore, the discussion that follows, is limited to this region.

The RCS of an object depends upon:

1. The size of the object.
2. The frequency of the transmitted waves.
3. The orientation of the object with respect to the antenna (viewing angle).
4. The material of the object, and
5. The polarization of the transmitted waves.

The radar cross-section is independent of the distance between the antenna and the target as long as the object is in the far field.

The critical parameter in the Rayleigh region is the volume of the scattering object. The object of interest may be replaced by an equivalent spheroid of the same volume and elongation. For a spheroid, with semi-axes a,a,b; the backscattering cross-section is given by (Crispin and Maffett, 1965),

$$\sigma = \frac{4}{\pi} k'^4 V^2 F^2 [1 + \frac{1}{\pi y} e^{-y}]^2 \qquad (3.10)$$

where, σ is the radar cross-section in m^2, $k' = 2\pi/\lambda$, λ is the free space wavelength in m, V is the volume of the object in m^3, F is the shape factor, and $y = b/a$.

Except for very flat oblate spheroids, the term in the brackets can be neglected.

The shape factor, F, is equal to

$$F_{\text{horz. Pol.}} = \frac{1}{2}\left[\frac{1}{2-L} + \frac{\cos^2\theta}{L} + \frac{\sin^2\theta}{2-2L}\right]$$

$$F_{\text{vert. Pol.}} = \frac{1}{2}\left[\frac{1}{L} + \frac{\cos^2\theta}{2-L} + \frac{\sin^2\theta}{2-2L}\right]$$

and

$$L_{\text{prolate spheroide}} = \frac{1}{c'^2} - \frac{1-c'^2}{2c'^3} \ln\frac{1+c'}{1-c'}$$

where, the semi-axes are $a, a, \frac{a}{\sqrt{1-c'^2}}$

$$L_{\text{oblate spheroide}} = \frac{\sqrt{1-c'^2}}{c'^3}\sin^{-1}c' - \frac{1-c'^2}{c'^2}$$

where, the semi-axes are $a, a, a\sqrt{1-c'^2}$

$$L_{\text{sphere}} = \frac{2}{3}$$

For a sphere, F, at all polarizations and viewing angles, is constant and is equal to 1.125.

The radar cross-section for the bistatic radar can be calculated from Eq. (5.9) by substituting F as follows (Crispin and Siegel, 1968):

$$F_{\text{horz, pol.}} = \frac{1}{2}\left[\frac{1}{2-L} + \frac{\cos\theta_r \cos\theta_t}{L} + \frac{\sin\theta_r \sin\theta_t}{2-2L}\right]$$

$$F_{\text{vert pol.}} = \frac{1}{2}\left[\frac{1}{L} + \frac{\cos\theta_r \cos\theta_t}{2-L} + \frac{\sin\theta_r \sin\theta_t}{2L}\right]$$

where, θ_r and θ_t represent the viewing angles of the receiver and transmitter, respectively. It is assumed that the transmitter, receiver and scattering object are coplanar.

In this chapter, an attempt was made to discuss some of the basic concepts, which establish theoretical background for the discussion that

follows. The equations derived in Chapter 5 are either modifications or extensions of the basic equations presented in this chapter.

CHAPTER 4

EXPERIMENTAL PROCEDURES

4.1 Introduction

Experiments were performed, both with single scattering targets and multiple scattering targets, to determine quantitatively the capabilities and limitations of the MDEF. Different types of seeds and metallic spheres of various diameters were used as single scattering targets. Rapeseeds and wheat were used in continuous flow experiments. The experiments were conducted in waveguides and in free space. The last configuration included both the monostatic and bistatic systems.

4.2 Sensing and Signal Processing Units

4.2.1 General Description of the System

The MDEF utilizes a commercially available Doppler module as a main sensing element. The output signal is amplified and displayed or recorded by an indicating unit. A general view of the sensing and signal processing units is shown in Fig. 4.1.

In all experiments performed in the monostatic configuration, a commercially available microwave Doppler transceiver, model MA-86105 (Microwave Associates), was used. It operated at a frequency of 10.525 GHz. A standard waveguide horn, Narda model 640, was used as an antenna. The transceiver contained an MA-49104 Gunn diode and an MA-40642 low noise Shottky mixer diode having the Noise Figure of 7.5 dB and the conversion losses of 5 dB. A waveguide ferrite circulator isolated the outgoing and incoming signals. The generator required a typical power supply of 10 V (DC) and had an output power of 25 mW.

In the waveguide configuration, an equipment similar to a wave-

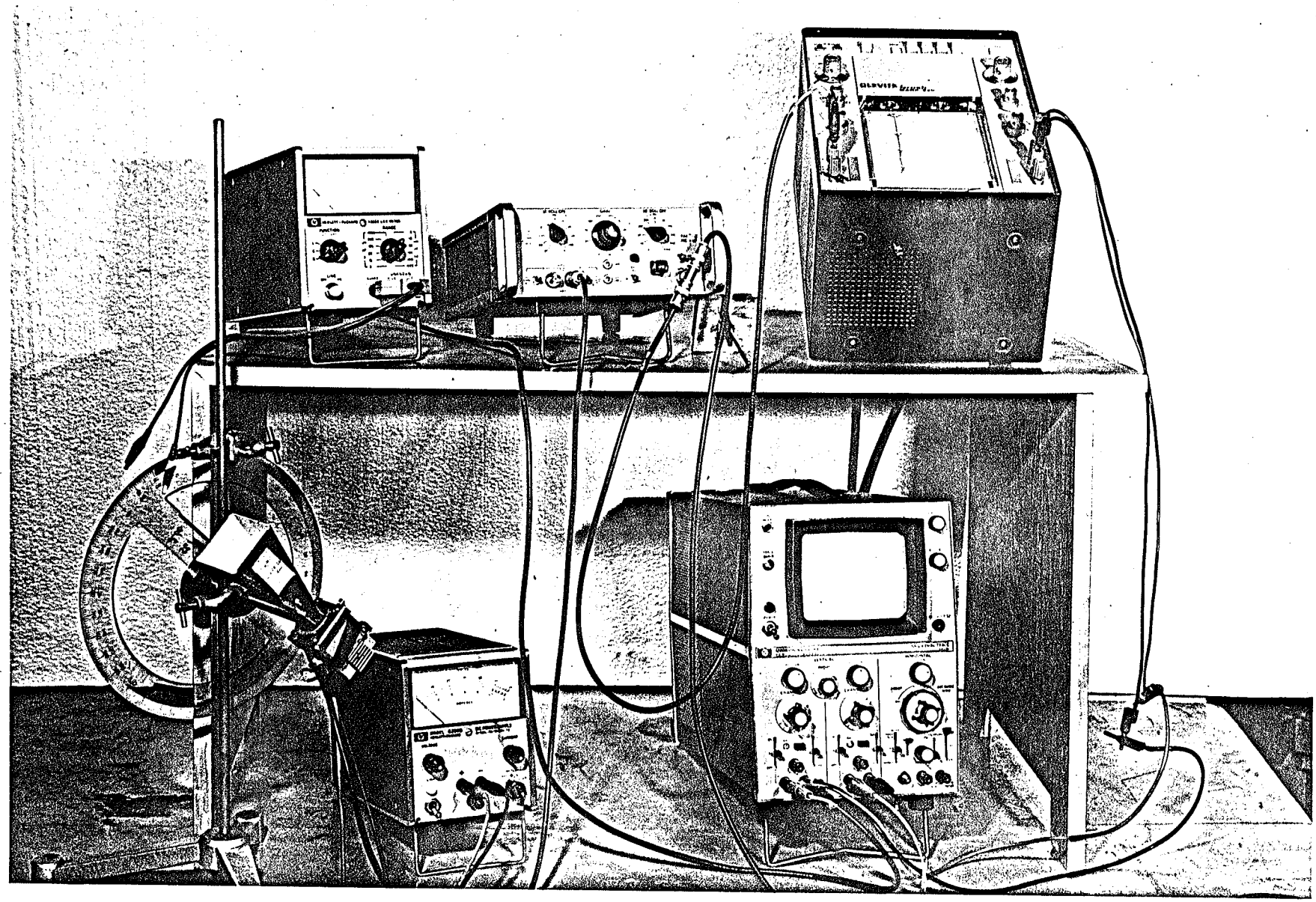

Fig. 4.1 General View of the Sensing and Signal Processing Units

guide noise generator mount was used. It contained a section of a WR-90 waveguide terminated with a matched load and an 0.008 m circular tube intersecting the waveguide at an angle of 10.5°. In these experiments, the transceiver was directly attached to the waveguide and the target was passing through the circular tube.

In the bistatic configuration, an additional waveguide detector mount, with an MA-40642 Shottky diode and a separate antenna Narda model 640, was used for the reception of the signal.

In the free space configuration, absorbing mats were used to screen the target from the surrounding and to minimize the stray reflections.

The Doppler module was supplied from an HP 6220B power supply. The signal from the mixer was amplified by a PAR 113 pass-band amplifier and further displayed or stored on the screen of an HP 1200 or Tektronix 564B storage oscilloscope. An HP 198A oscilloscope camera was used for taking photographs of the signal. A Clevite Mark 220 recorder was used for continuous recording of the signal. In the continuous flow experiments, the signal was processed by an analog frequency meter.

4.2.2 Viewing Angle

In all the experiments in the free space configuration, the viewing angle was defined as the angle between the electrical axis of the antenna and the velocity vector. A large circular protractor was attached to the Doppler module to measure this angle. The protractor rotated with the Doppler radar in the plane of observation of the target. The viewing angle was read from the protractor against a fixed indicator.

4.2.3 Target Position Indicator

A light sensitive photoresistor system was used as a target position indicator. A light beam from a collimated light source was

focussed on the photoresistor through a tube with a narrow horizontal slit. The moving target affected the illumination of the photoresistor. The resulting change in resistance was detected by an HP 4332LCR meter and recorded in the second channel of the recorder as a sharp pulse. The pulses received from the position indicator were utilized to determine the position of the scattering targets and to measure their actual velocity.

4.3 Experimental Set-Up

4.3.1 Single Scattering Objects

Free Space Configuration: A schematic diagram of the experimental set-up employed in the free space experiments is shown in Fig. 4.2. The experiments were performed using a band saw frame as a target moving system. Large band saw pulleys did not stress the delicate band appreciably and moved the target smoothly at a fairly constant speed. The pulleys were driven by a variable speed electric motor.

The experiments were performed using a wide endless nylon ribbon as a target carrier. When the gain of the amplifier was set properly and the viewing plane was adjusted to be perpendicular to the direction of the movement of the ribbon, the reflections from the ribbon were negligible. Metallic spheres and different seeds were glued to the ribbon at precisely measured distances. The arrangement of scattering objects is shown in Fig. 4.3. The experiments were performed at various speeds, and at different viewing angles and distances. A photograph of the experimental set-up is shown in Fig. 4.4, while the target position indicator is shown in Fig. 4.5.

Waveguide configuration for experimental set-up is shown

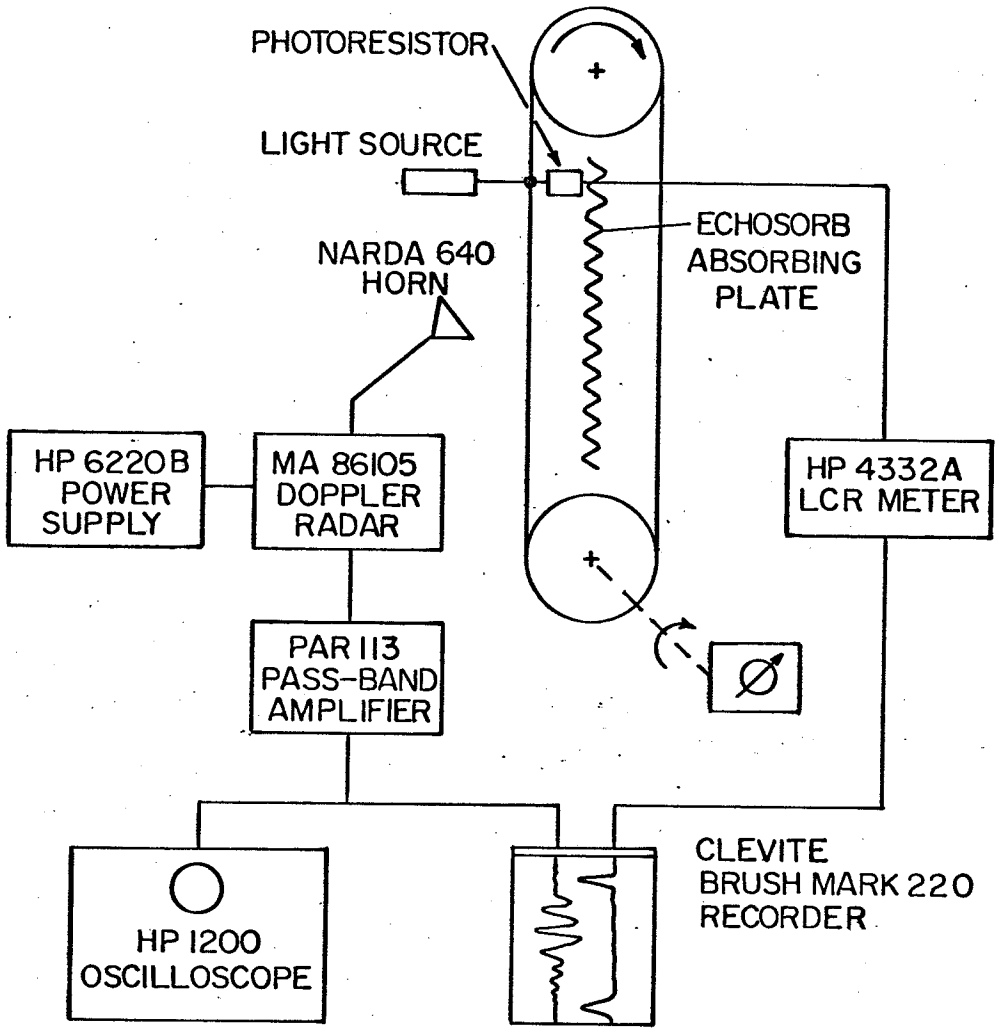

Fig. 4.2 Schematic Diagram of the Experimental Set-Up for Single Scattering Particles

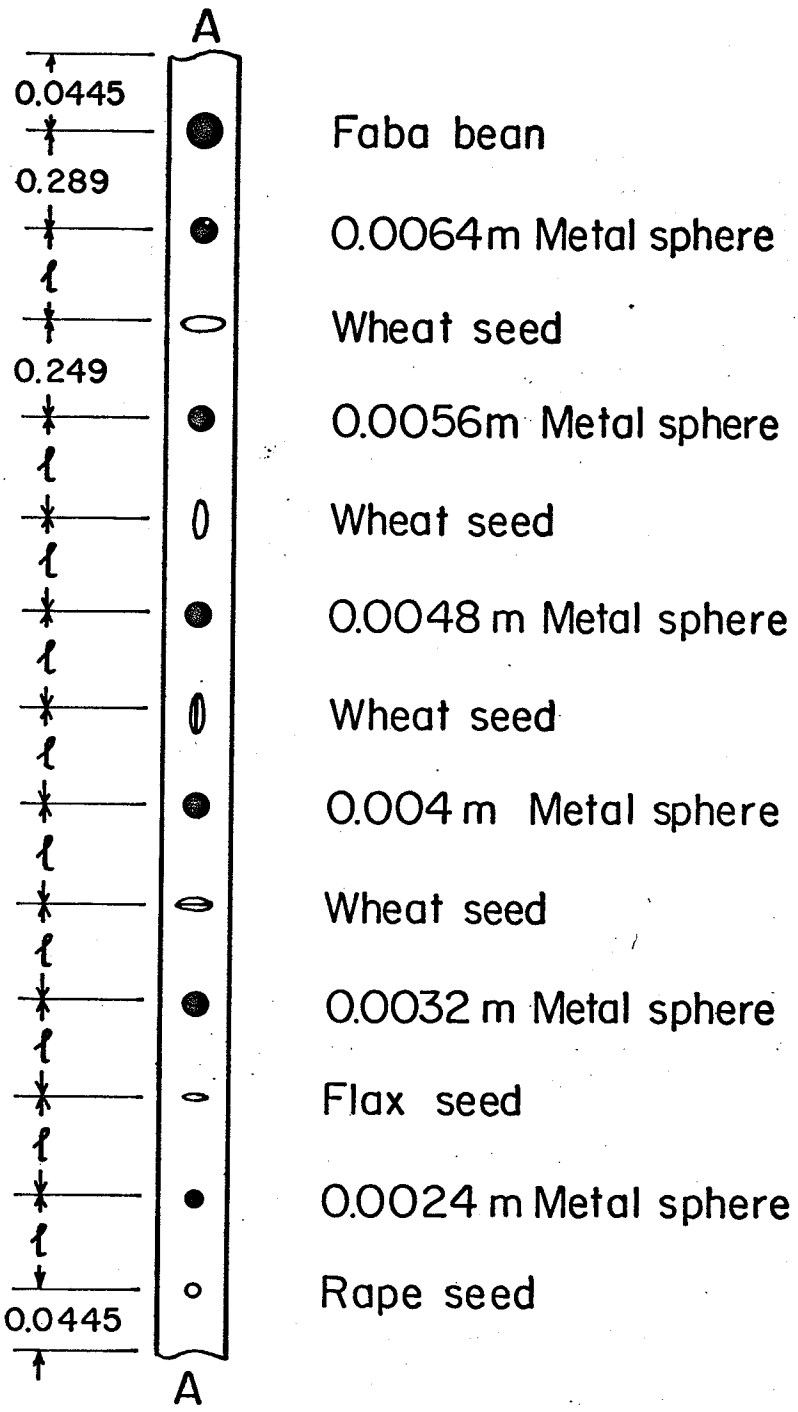

Fig. 4.3 Arrangement of the Scattering Particles in the Free Space Configuration

[Distances are measured from the axes of the targets, ℓ = .252 m.]

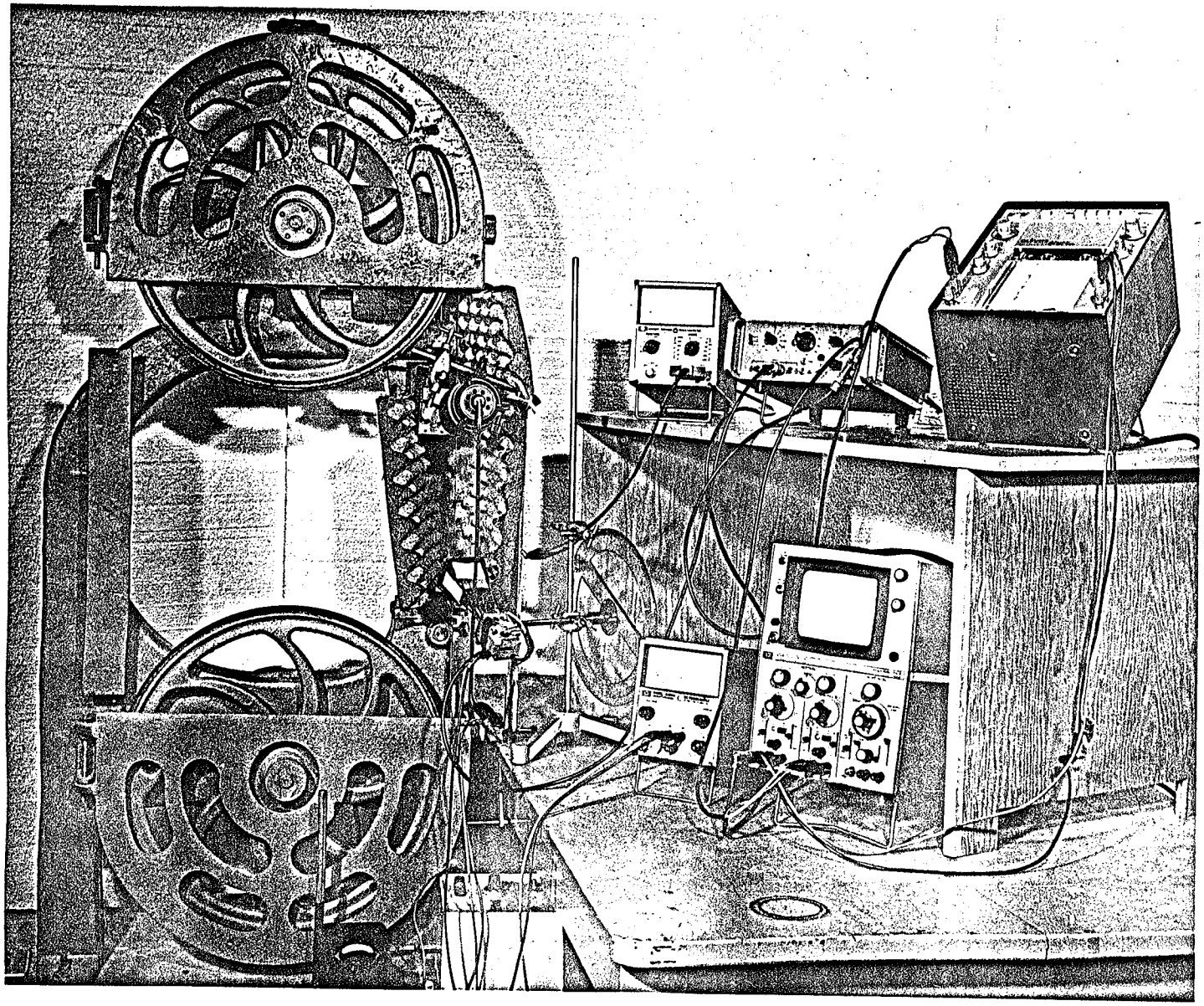

Fig. 4.4 General View of the Experimental Set-Up for Single Scattering Particles in the Free Space Configuration

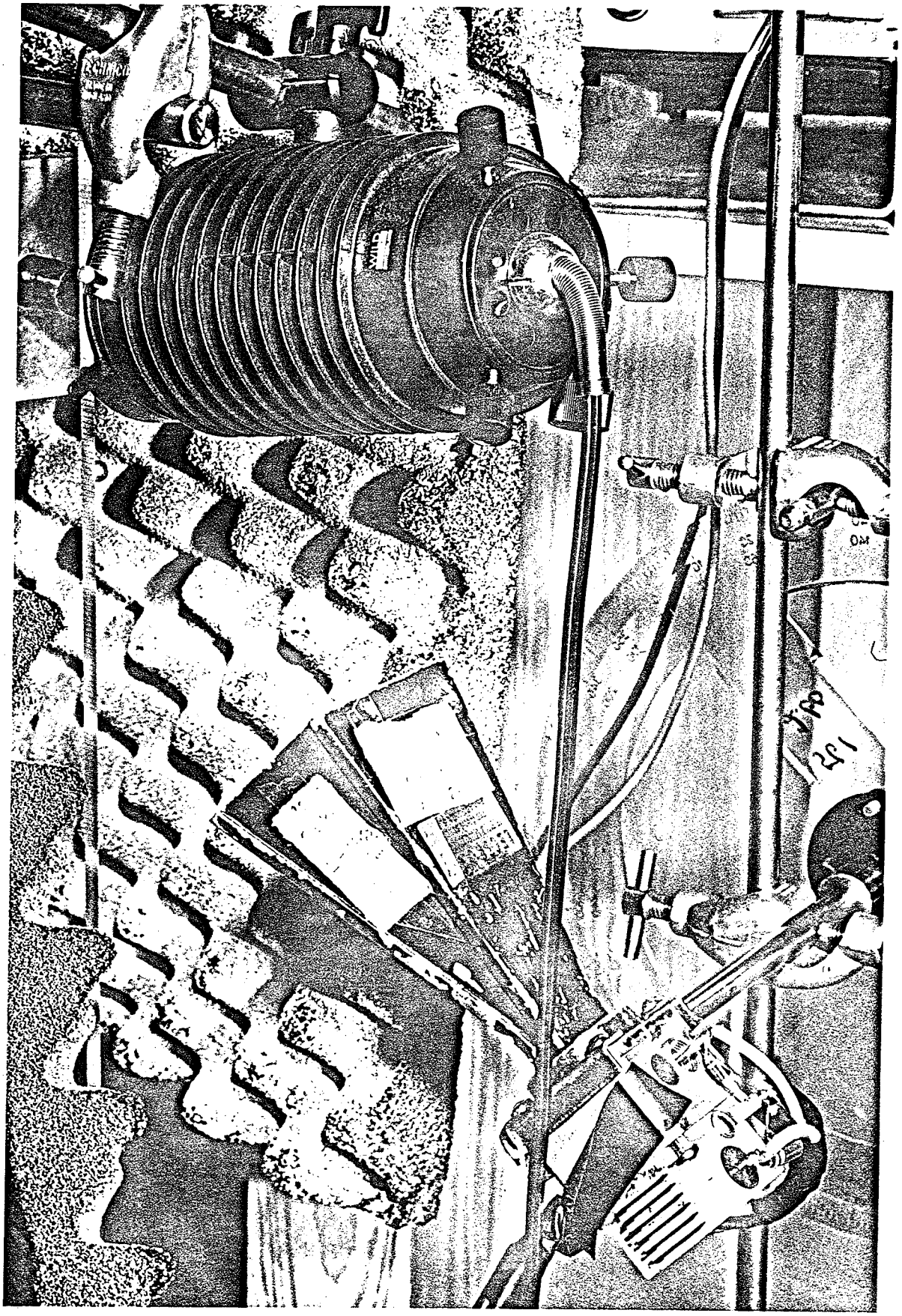

Fig. 4.5 Target Position Indicating System

Waveguide Configuration: An experimental set-up for the waveguide configuration is shown in Fig. 4.6. The nylon ribbon supporting the scattering objects passed through a circular tube intersecting with a section of the rectangular waveguide. The arrangement of metal spheres and seeds on the ribbon is shown in Fig. 4.7.

4.3.2 Continuous Flow Experiments

Gravity flow was employed in all the experiments with continuous flow of particulate solids. The overall view of the experimental set-up is shown in Fig. 4.8. The test material fell by gravity from a large hopper through a section of plastic pipe to a collecting bucket located underneath. The size of the opening in the hopper was designed to accomodate pipes of various diameters. A shutter at the bottom of the hopper allowed starting or stopping the material flow.

Plastic rings with different bore sizes were used to obtain different flow rates in the centre of the pipe. The test material was collected in a large bucket and continuously lifted to the hopper by an auger conveyor. Above certain flow head in the hopper, which was determined experimentally, the flow remained practically independent of the variations in the flow head. A direct weighing and timing technique was used for calibration of the mass flow rate.

Rapeseeds and wheat were used as test materials, each in pipes of 0.044 m and 0.0635 m diameter.

The initial experiments were performed at different viewing angles and distances to determine the optimum viewing angle and distance. Further experiments were aimed at the determination of the relationship between the Doppler frequency and the flow rate, and were performed at a fixed viewing angle and distance. A simplified diagram of the complete

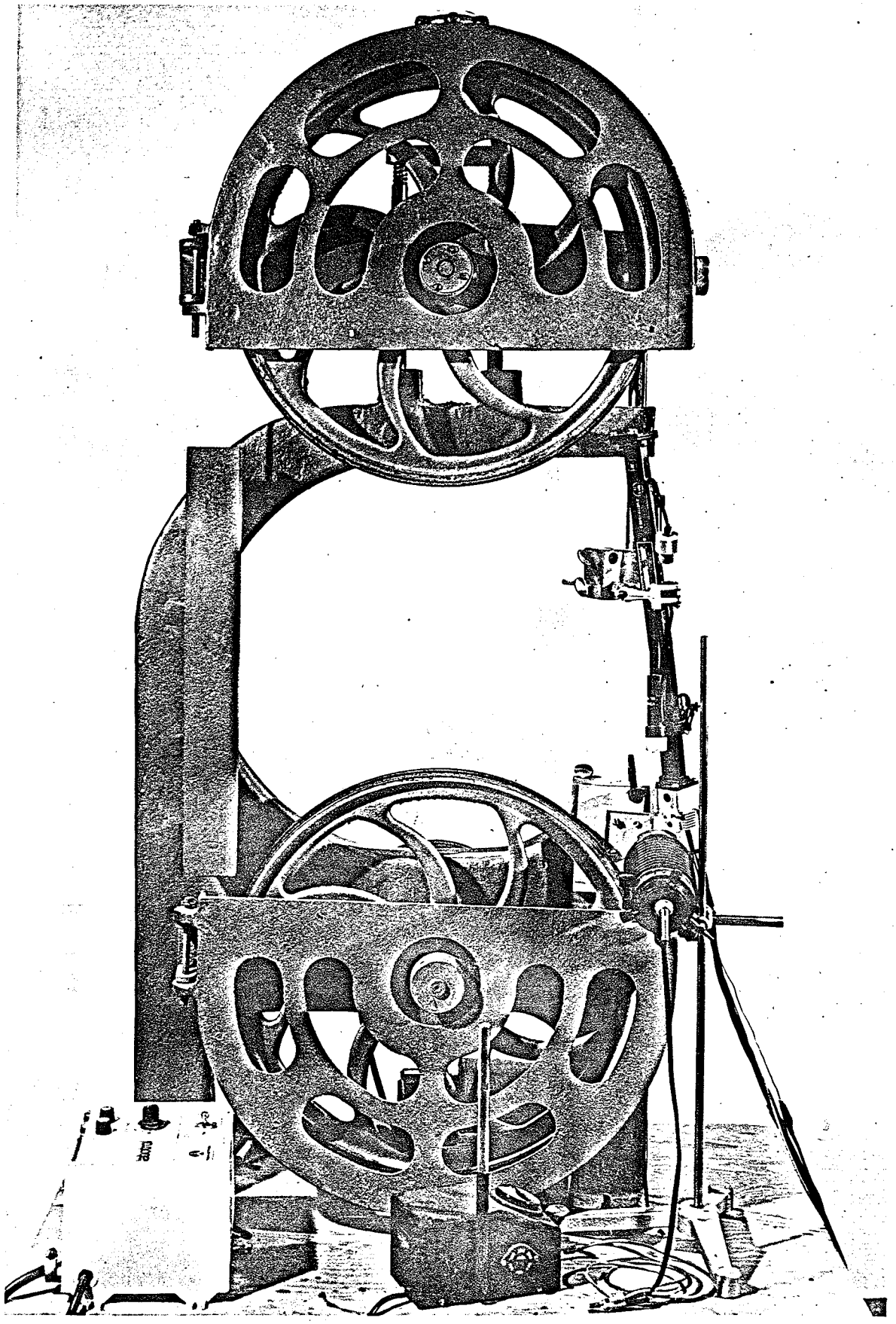

Fig. 4.6 Experimental Set-Up for Single Scattering Particles in the Waveguide Configuration

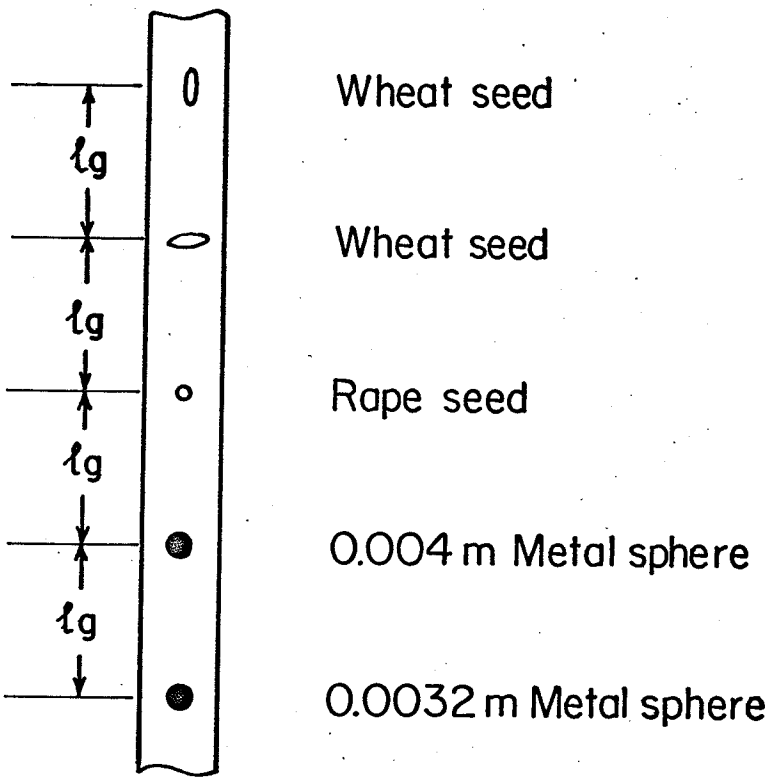

Fig. 4.7 Arrangement of the Scattering Particles in the Waveguide Configuration

[Distances are measured from the axes of the targets, ℓ_g = 0.2 m]

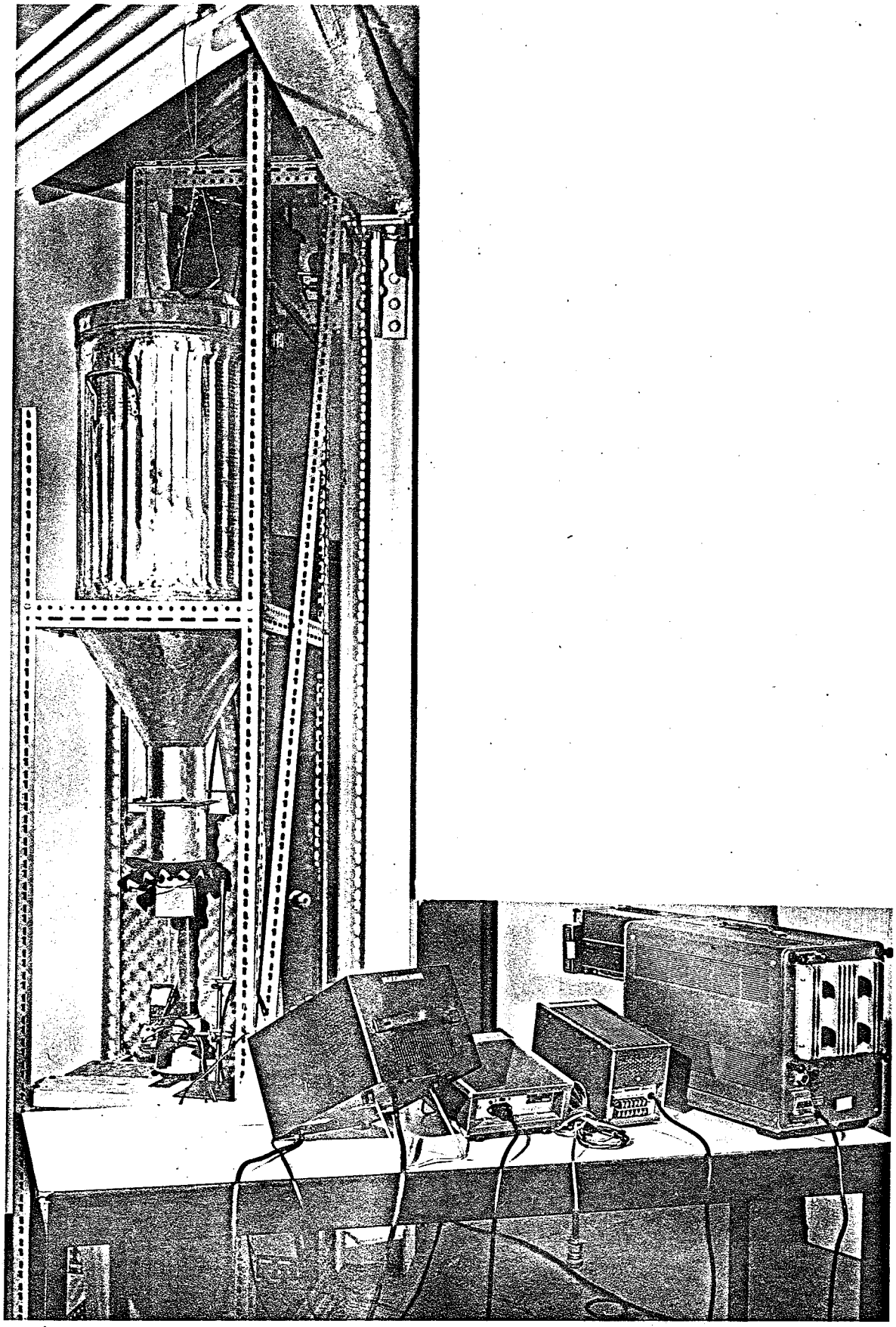

Fig. 4.8 General View of the Experimental Set-Up for Continuous Flow of Granular Materials

experimental set-up is shown in Fig. 4.9.

The experiments in the waveguide configuration were performed with rapeseeds only. Fig. 4.10 shows an experimental set-up used in those experiments.

The experiments in the bistatic configuration were performed at different angles between the receiver and transmitter. An experimental set-up ulilized in the bistatic configuration is shown in Fig. 4.11.

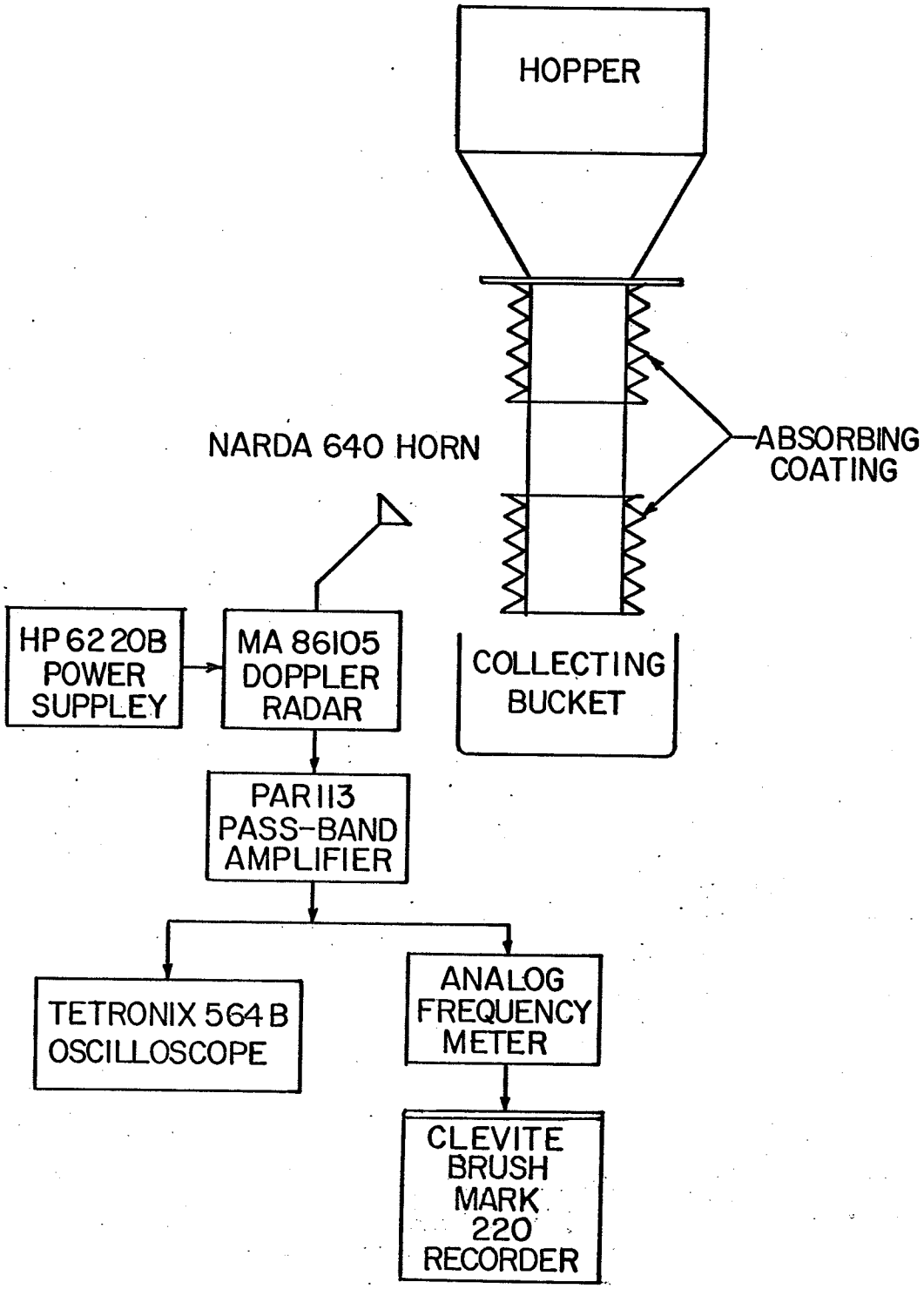

Fig. 4.9 Experimental Set-Up for Continuous Flow Experiments in the Monostatic Configuration

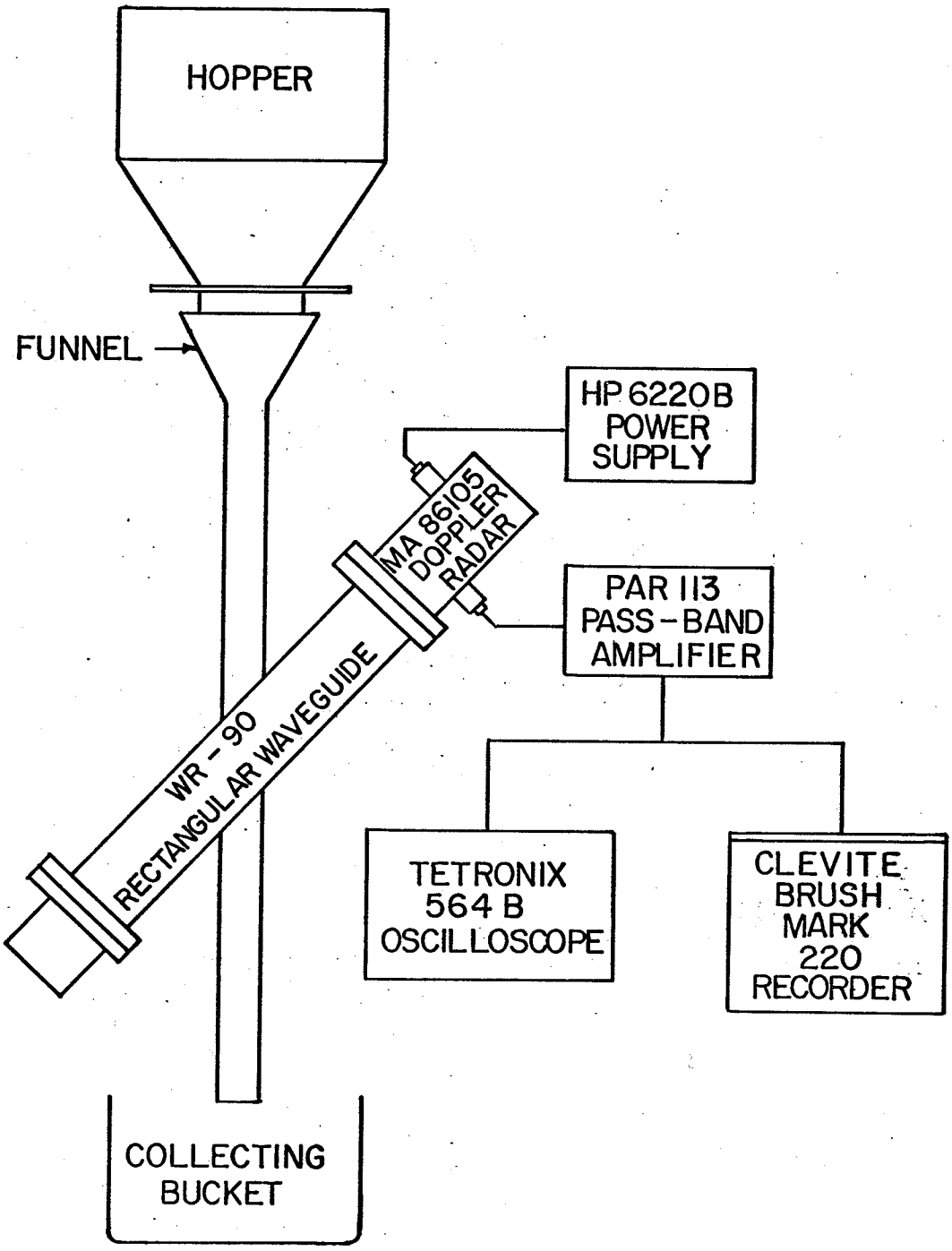

Fig. 4.10 Experimental Set-Up for Continuous Flow Experiments in the Waveguide Configuration

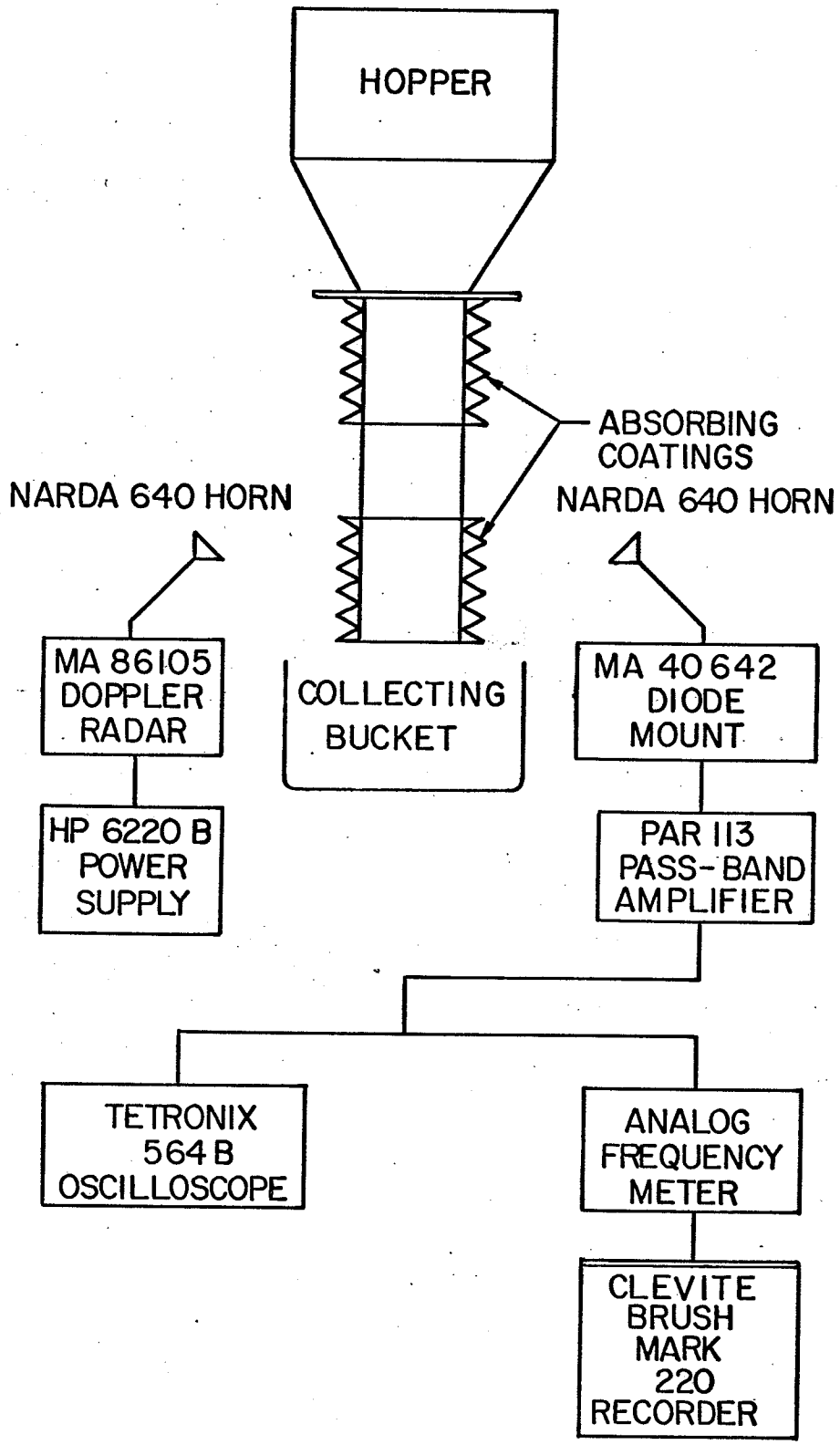

Fig. 4.11 Experimental Set-Up for Continuous Flow Experiments in the Bistatic Configuration

CHAPTER 5

RESULTS AND DISCUSSION

5.1 Single Scattering Particles in the Free Space Configuration

5.1.1 Doppler Frequency Spectrum

Fig. 5.1 shows typical recordings of the Doppler signals from single particles moving at a constant velocity. The received Doppler signal is not of one discrete frequency as would normally be expected for a particle moving at constant velocity. All the practical antennas, used to radiate and receive the microwave energy, have a certain definite beamwidth. This implies that the angle θ in Eq. (3.1) is different for different viewing angles within the antenna beam. As the target takes a finite time to cross the antenna beam, the return signal comes at different angles. Therefore, the Doppler signal does not have any single discrete frequency, but is spread over a certain frequency band. This problem is well known in navigation where a spread of Doppler frequency has been reported by Berger (1957), Ehrman (1964) and Pawla (1968).

In particular, the Doppler frequency associated with the angle θ_i is given by

$$f_{d_i} = 2f_o/c \; v \cos\theta_i \tag{5.1}$$

and is spread over the bandwidth

$$\Delta f_d = 2f_o/c \; v(\cos\theta_h - \cos\theta_\ell) \tag{5.2}$$

where θ_h and θ_ℓ are the angles associated with the Doppler signal returned from the extremes of the antenna beam.

Eq. (5.2) may be further expanded as follows:

$$\Delta f_d = \frac{2f_o}{c} \; v \; [2\sin(\frac{\theta_h + \theta_\ell}{2}) \; \sin \; (\frac{\theta_h - \theta_\ell}{2})]$$

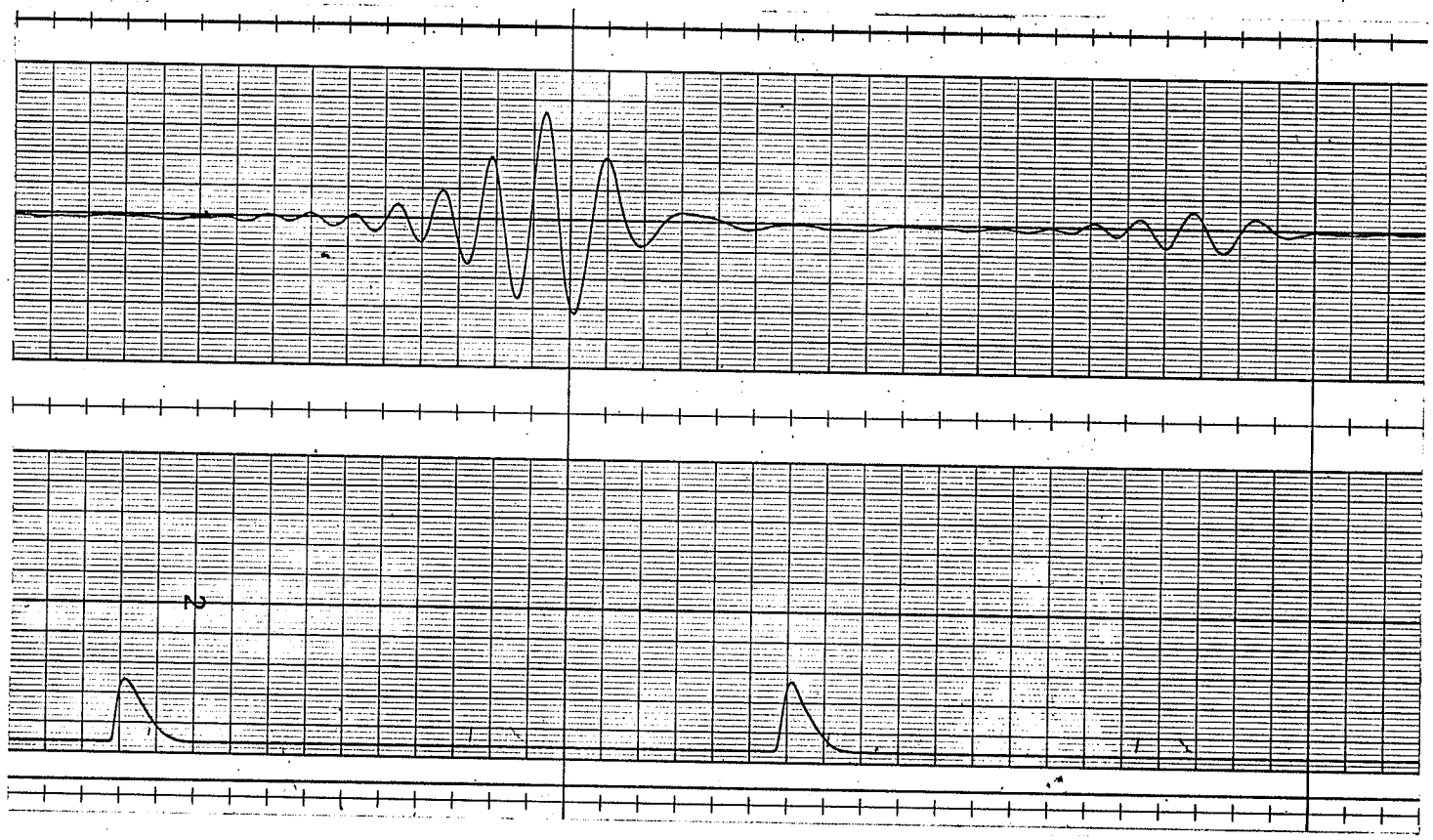

Fig. 5.1 Typical Recordings of the Doppler Signals for Single Scattering Particles in the Free Space Configuration

[Channel 1: Signals from the Doppler Radar Channel 2: Pulses from the Photoresistor
Viewing angle = 45° Chart speed = 0.125 m/s Sensitivity of the recorder = 200 mV/div
Grain of the amplifier = 1000 V/V]

$$\simeq \frac{2f_o}{c} v \sin\theta_o \cdot \Delta\theta \qquad (5.3)$$

where, θ_o is the axial viewing angle, and $\Delta\theta$ is the antenna beamwidth in the plane of motion of the target in radians.

5.1.2 Doppler Frequency and Amplitude Variations

The frequency and amplitude of the Dopplerd signals have been plotted in Figs. 5.2, 5.3 and 5.4 as a function of the target position across the antenna beam. The maximum amplitude of the signal did not, necessarily, occur at the electrical axis of the antenna, but the deviations were very small. Therefore, for simplicity, the position of the target was calculated from the point of maximum amplitude.

According to the approximation given in Eq. (5.3), the bandwidth of the Doppler signal is a function of θ_o, $\Delta\theta$, and v. Similar behaviour has been reported by Ehrman (1964) for the Doppler radar used in navigation. He found the Doppler signal to be a function of: the two way antenna pattern, the orientation of antenna with respect to the terrain, the angle between the antenna beam and velocity vector, and the terrain backscattering characteristics.

The amplitude of the signal varies due to the variations in the distance to the target and the intensity of radiation which depends upon the antenna pattern. The amplitude of the signal increases as the target approaches the antenna axis. The peak of the signal occurs in the region where the ratio of radiation intensity to the fourth power of range is maximum. It decreases again as the target recedes, because of decreasing radiation intensity off the antenna axis.

5.1.3 Relationship between the Velocity and Doppler Frequency

The spectrum of the received signal can be assumed (Ehrman, 1964)

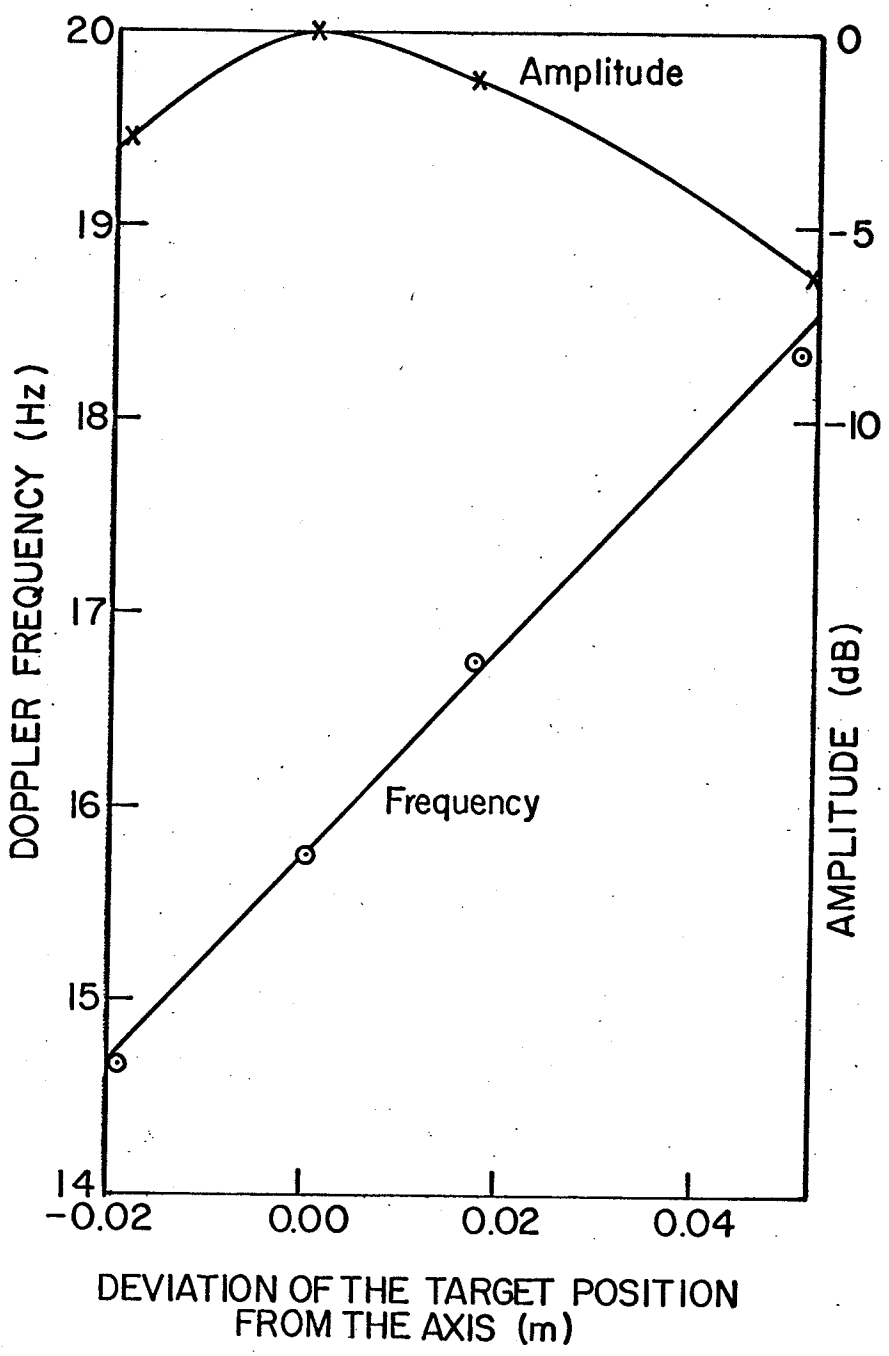

Fig. 5.2 Variation of the Amplitude and Doppler Frequency for a Wheat Seed Moving Across the Antenna Beam. The Major Axis of the Seed was Parallel to the Plane of Polarization.

[Velocity of the seed = 0.28 m/s Viewing angle = 30°]

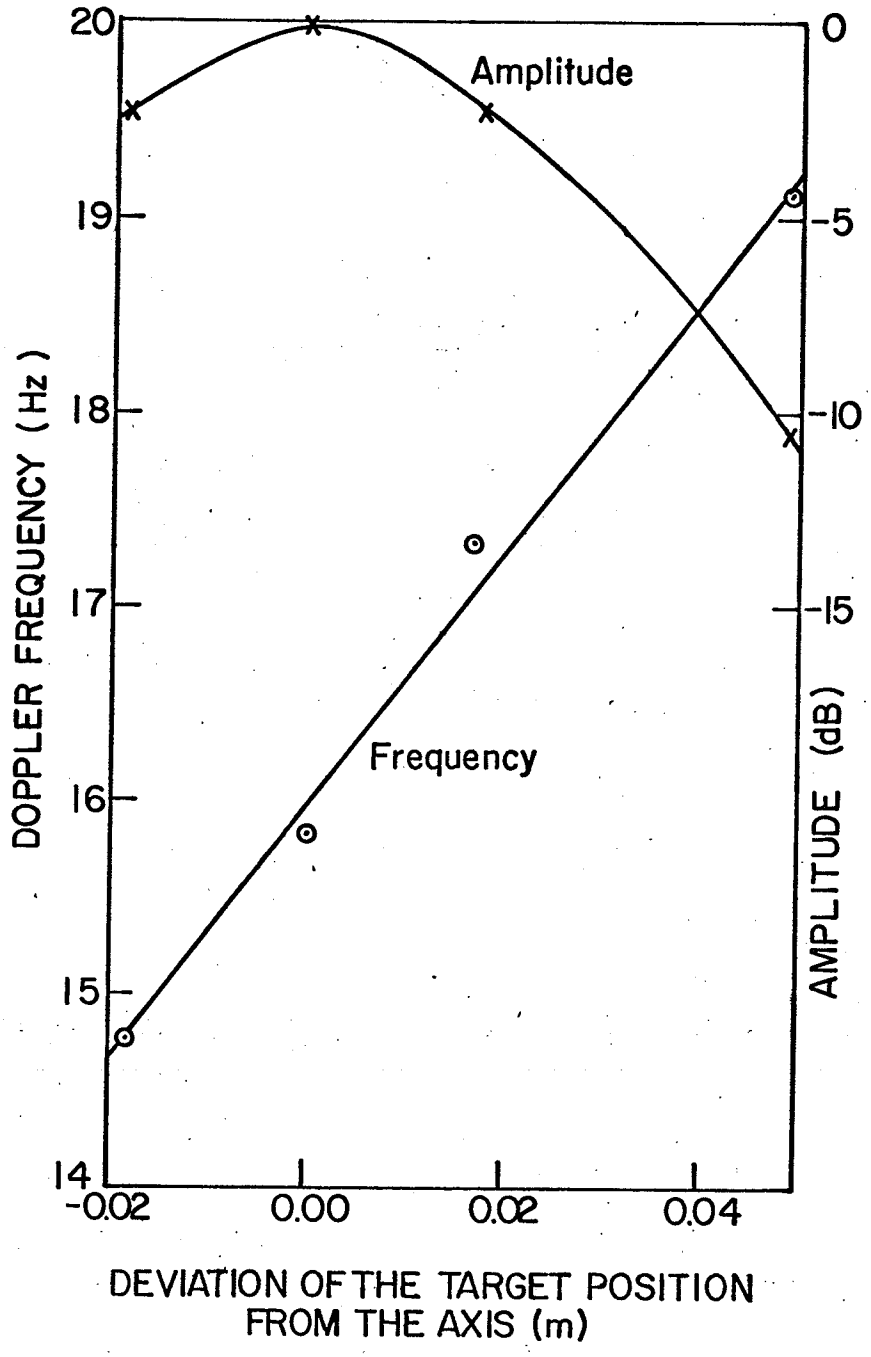

Fig. 5.3 Variation of the Amplitude and Doppler Frequency for a Wheat Seed Moving Across the Antenna Beam. The Major Axis of the Seed was Perpendicular to the Plane of Polarization.

[Velocity of the seed = 0.28 m/s Viewing angle = 30°]

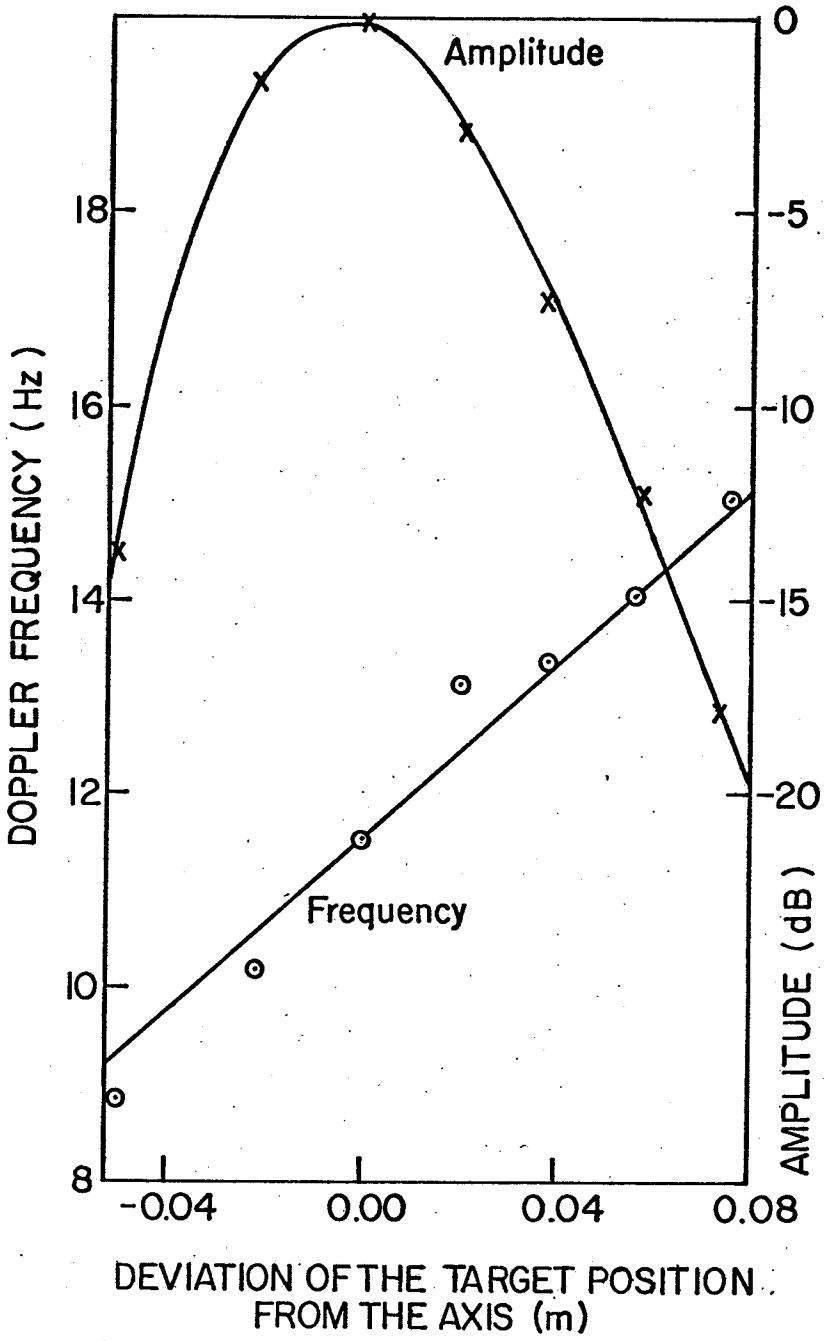

Fig. 5.4 Variation of the Amplitude and Doppler Frequency for a 0.004 m Metal Ball Moving Across the Antenna Beam

[Velocity of the ball = 0.24 m/s Viewing angle = 45°]

to be centered around $f_o \pm \overline{f}_d$, where f_o is the transmitted frequency and $\overline{f}_d$ is the mean Doppler frequency. Although it was found (also, reported by Edward et al., 1970 for laser velocitimeters) that $\overline{f}_d$ did neither correspond exactly to the electrical axis of the antenna nor to the peak point, the velocity calculated by substituting $\overline{f}_d$ and θ_o in Eq. (3.2) is a good approximation of the actual velocity. Thus, Eq. (3.2) can be modified as

$$v = \frac{d}{2f_o} \overline{f_d} / \cos(\theta_o) \qquad (5.4)$$

where, $\overline{f}_d = 1/N \sum_{i=1}^{N} f_{d_i}$

and θ_o is the axial viewing angle.

In Fig. 5.5, the radial velocity is plotted versus the mean Doppler frequency. Most of the experimental points lie very close to the theoretical straight line calculated from Eq. (5.4).

A comparison of the velocities, calculated from Eq. (5.4) and those calculated from the photoresistor pulses, is shown in Table 5.1.

The mean Doppler frequency, $\overline{f}_d$ in Table 5.1 was determined by averaging the instantaneous frequencies calculated from their time periods. This method is similar to the well known zero crossing technique of frequency counting in a certain period of time. The method has been suggested and analysed by Ehrman (1964), Pawla (1968) and Kobayashi et al. (1974). In Table 5.2, the mean Doppler frequency was calculated by dividing the total number of waves of the Doppler signal by their cummulative time period. The velocities indicated by the Doppler radar are in good agreement with those calculated from the photoresistor pulses. The difference between the two velocities, listed in Tables 5.1 and 5.2, is not more than 5% for most of the observation points.

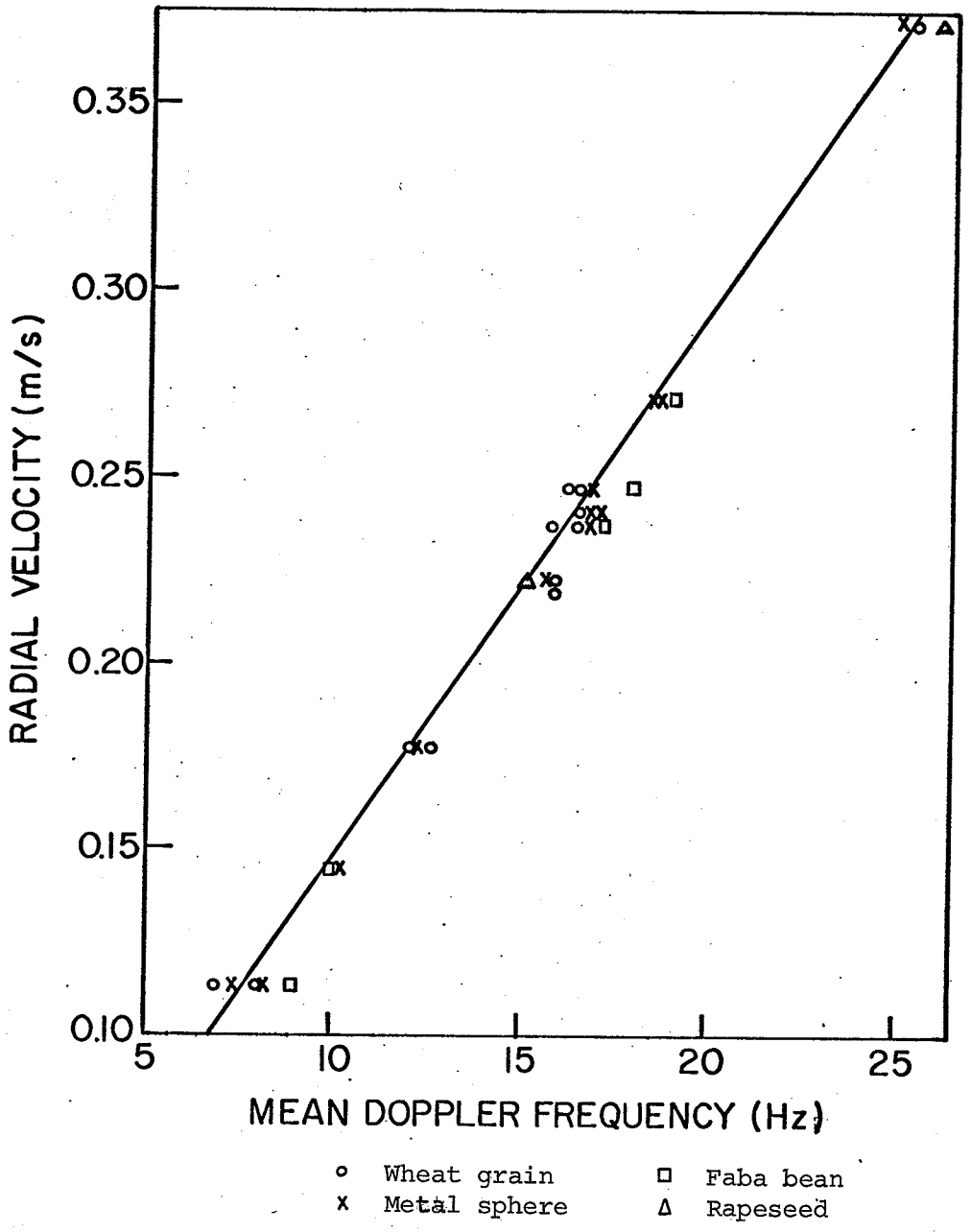

Fig. 5.5 Radial Velocity vs Mean Doppler Frequency for Single Scattering Particles in the Free Space Configuration

[Radial velocity = $v_a \cos\theta_o$, where v_a is the velocity calculated from photoresistor pulses and θ_o is the axial viewing angle]

Table 5.1

Comparison of Velocities Calculated from Eq. (5.4) and from the Photoresistor Pulses in the Free Space Configuration

	$\overline{f_d}$ (Hz)	Velocity from Eq. (5.4) (m/s)	Velocity from Photoresistor (m/s)	Difference (%)
Wheat*	Angle 30°			
Wheat**	16.5	0.271	0.279	2.87
Wheat**	16.8	0.276	0.280	1.42
Metal ball 0.004 m	17.2	0.283	0.280	-1.07
0.0032mm	16.6	0.273	0.274	0.40
	Angle 45° (Lower velocity)			
Wheat*	12.7	0.256	0.249	-2.81
Wheat**	12.2	0.249	0.243	-2.47
Metal ball 0.004 m	12.3	0.248	0.243	-2.06
0.0032 m	12.7	0.256	0.250	-2.40
	Angle 45° (higher velocity)			
Wheat*	27.5	0.554	0.527	-5.12
Wheat**	25.4	0.512	0.527	2.85
Metal ball 0.004 m	27.6	0.556	0.526	-5.70
0.0032 m	26.8	0.540	0.526	-2.66
Rapeseed	26.2	0.528	0.526	-0.38
	Angle 55°			
Wheat*	15.8	0.392	0.387	-1.29
Wheat**	15.7	0.390	0.382	-2.01
Metal ball 0.004 m	16.3	0.405	0.382	-6.00
0.0032 m	15.7	0.390	0.388	-0.52
Rapeseed	15.2	0.378	0.388	2.57

Table 5.1

Legend

* The major axis of the seed parallel to the plane of polarization

** The major axis of the seed perpendicular to the plane of polarization

5.1.4 Effect of the Viewing Angle

Experimental results of velocities, indicated by the Doppler radar, did not show any significant difference for different viewing angles varying from 30° to 60°. Large dispersion of some experimental points at the viewing angle of 60° (Table 5.2) can be attributed to experimental errors. It will be explained in section 5.1.5 how the experimental uncertainties increase at large viewing angles.

Table 5.2

Comparison of the Velocities Measured by the Doppler Radar and by the Photoresistor in the Free Space Configuration (the Doppler frequency calculated by counting the number of waves in a certain period of time)

	$\bar{f}_d$ (Hz)	Velocity measured by the Doppler radar (m/s)	Velocity measured by the Photoresistor (m/s)	Difference (%)
	$\theta_o = 45°$			
Faba bean	18.2	0.367	0.350	-4.86
Wheat*	16.4	0.331	0.350	5.43
Wheat**	16.7	0.336	0.350	4.00
Wheat†	17.3	0.349	0.350	0.29
Wheat††	16.9	0.341	0.350	2.57
Metal ball				
0.0048 m	18.1	0.365	0.350	-4.29
0.0040 m	16.9	0.341	0.350	2.57
0.0032 m	17.2	0.347	0.350	0.86
	$\theta_o = 50°$			
Faba bean	17.4	0.386	0.369	-4.61
Wheat**	15.8	0.350	0.369	5.15
Wheat*	16.5	0.366	0.369	0.81

Table 5.2 - Continued

	$\overline{f}_d$ (Hz)	Velocity measured by the Doppler radar (m/s)	Velocity measured by the Photoresistor (m/s)	Difference (%)
Wheat†	17.4	0.386	0.369	-4.61
Wheat††	16.1	0.357	0.369	-3.25
Metal ball				
0.0056 m	17.4	0.386	0.369	-4.61
0.0048 m	16.8	0.372	0.369	-0.81
0.0040 m	16.9	0.375	0.369	-1.62
0.0032 m	16.7	0.370	0.369	-2.71
	θ_o = 60°			
Faba bean	8.6	0.245	0.23	-6.52
Wheat*	7.2	0.205	0.23	10.8
Wheat**	8.6	0.245	0.23	-6.52
Wheat†	8.0	0.228	0.23	0.86
Wheat††	8.1	0.231	0.23	0.44
Metal ball				
0.0064	8.6	0.245	0.23	-6.52
0.0056	8.4	0.239	0.23	-3.91
0.0048	7.7	0.219	0.23	4.78
0.0040	8.2	0.234	0.23	-1.73
0.0032	7.8	0.222	0.23	3.48

Table 5.2

Legend

* The major axis of the seed parallel to the plane of polarization and the crease facing towards the ribbon

** The major axis of the seed perpendicular to the plane of polarization and the crease facing towards the ribbon

† The major axis of the seed perpendicular to the plane of polarization and the crease facing up

†† The major axis of the seed parallel to the plane of polarization and the crease facing up

5.1.5 Experimental Uncertainty

There are two major sources of uncertainties in calculating the velocity from Eq. (5.4): the noise accompanying the signal and the errors in measurement of the viewing angle. In addition, the uncertainties occur due to non-ideal working of the system components. On the other hand, the response of the photoresistor depends upon the size and shape of the target and this may cause substantial error in calculating the actual velocity.

Noise: In addition to the random nature of the Doppler signal, it is always accompanied by noise. This complicates the problem of determining the mean frequency and has a bearing on the accuracy of the Doppler system output.

Assuming that the signal is large compared with noise, the error in the Doppler frequency due to noise is given by (Skolnik, 1962)

$$\delta f_d/f_d = \frac{1}{2\pi (S/N)^{1/2}} \qquad (5.5)$$

where $\delta f_d/f_d$ is the relative error and S/N is the signal-to-noise (power) ratio.

Thus, the relative error in calculating the velocity will decrease with an increase in signal-to-noise ratio.

Viewing Angle: If the viewing angle was $\theta_o + \delta\theta$, instead of θ_o, the velocity would be given by

$$v = \frac{c}{2f} \; f_d/\cos(\theta_o+\delta\theta)$$

while, the calculated velocity would be

$$v_c = \frac{c}{2f} \times f_d/\cos(\theta_o+\delta_\theta)$$

thus, the relative error

$$\frac{\Delta v}{v} = \left[\frac{1}{\cos(\theta_o + \delta\theta)} - \frac{1}{\cos\theta_o} \right] \cos(\theta_o + \delta\theta)$$

When $\delta\theta$ is small, this reduces to

$$\frac{\Delta v}{v} \simeq \tan\theta_o \cdot \delta\theta \qquad (5.6)$$

where $\delta\theta$ is in radians. Thus, at the viewing angle of 45°, the deviation of one degree in θ_o would cause an error of approximately 1.7%. As θ_o increases, the velocity becomes highly sensitive to errors in θ_o due to the rapid increase of $\tan\theta_o$. For example, at the viewing angle of 60°, the deviation of one degree causes an error of approximately 3%.

5.1.6 RCS of Various Targets

The radar cross-sections of the various targets were calculated using the metallic calibrating spheres. Under similar conditions, the ratio of power received is

$$P/P_o = \sigma/\sigma_o$$

but $P/P_o = (E/E_o)^2$

therefore, $\sigma/\sigma_o = (E/E_o)^2 \qquad (5.7)$

where σ is the radar cross-section of the target in m^2, σ_o is the radar cross-section of the calibrating sphere in m^2, E is the maximum amplitude of the signal from the target in V and E_o is the maximum amplitude of the signal from the calibrating sphere in V.

Table 5.3 shows the experimental and theoretical values of the normalized RCS of several metal spheres, measured at different viewing angles. The cross-sections have been normalized with respect to the RCS

of a 0.004 m metal sphere. The experimental values of the normalized RCS show good agreement with the theoretical values calculated from Eq. (3.10). The slight discrepancies are due to the fact that the maxima of the amplitude of the Doppler signals do not, necessarily, correspond to the same point for all the spheres. This is clear from Fig. 5.6, where the curves are extrapolated to maxima for different spheres.

Table 5.3

Experimental and Theoretical Values of the Normalized RCS of Different Metal Spheres

Diameter (m)	Normalized RCS (σ/σ_o*)			
	Experimental			Theoretical
	45°	50°	60°	
0.0056	7.29	7.24	7.34	7.29
0.0048	3.24	2.92	3.17	2.89
0.0032	0.25	0.28	0.25	0.25
0.0024	0.04	0.056	0.044	0.04

* The RCS of a 0.004 m sphere

Amplitudes of the Doppler signals resulting from scattering by different dielectric particles are plotted as a function of time in Fig. 517. The curve for a 0.004 m metal sphere is also included as a reference. The RCS of various dielectric particles are listed in Table 5.4. The tabulated values were calculated from the relation

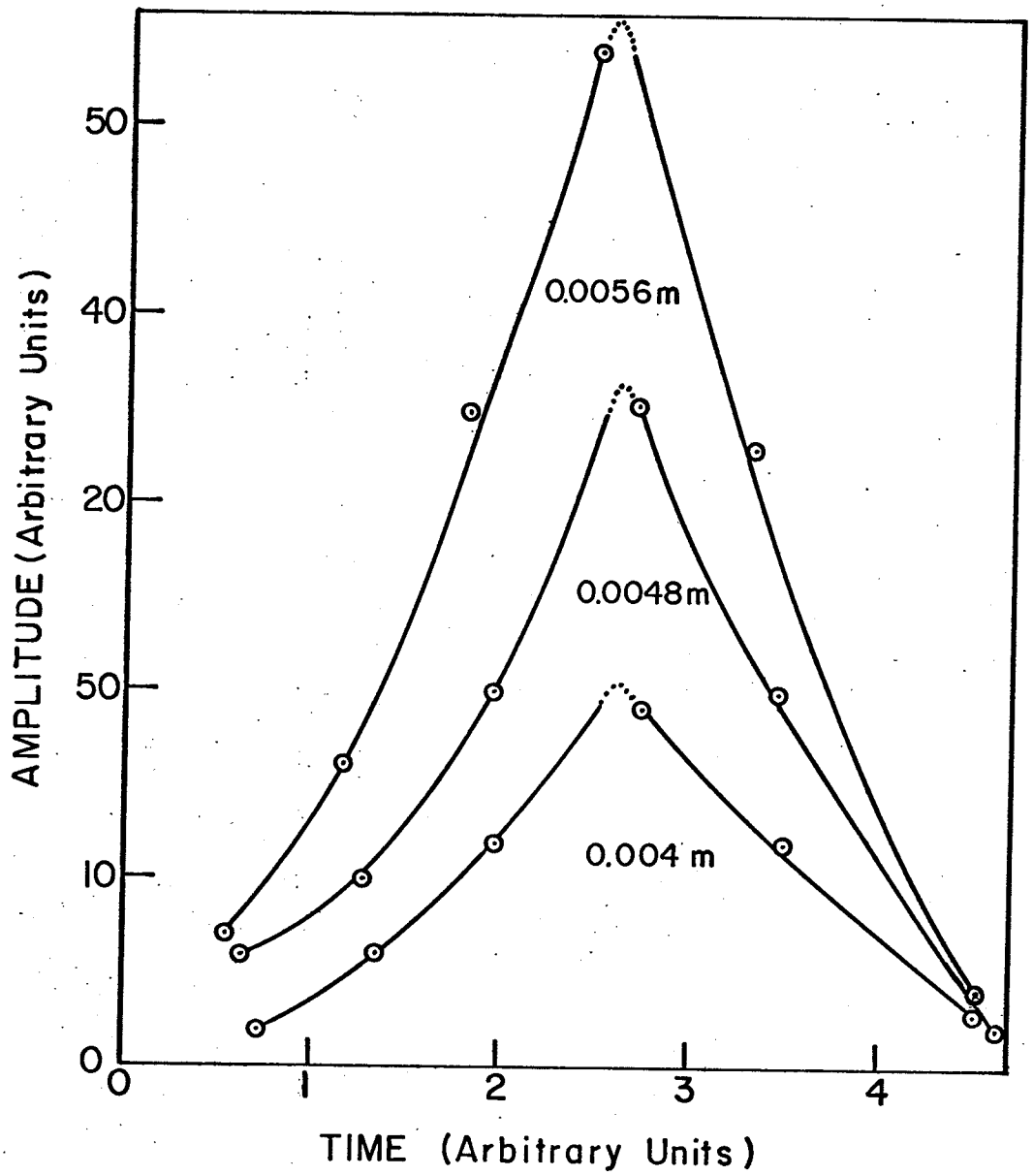

Fig. 5.6 Amplitude of the Doppler Signal as a Function of Time for Different Metal Spheres in the Free Space Configuration

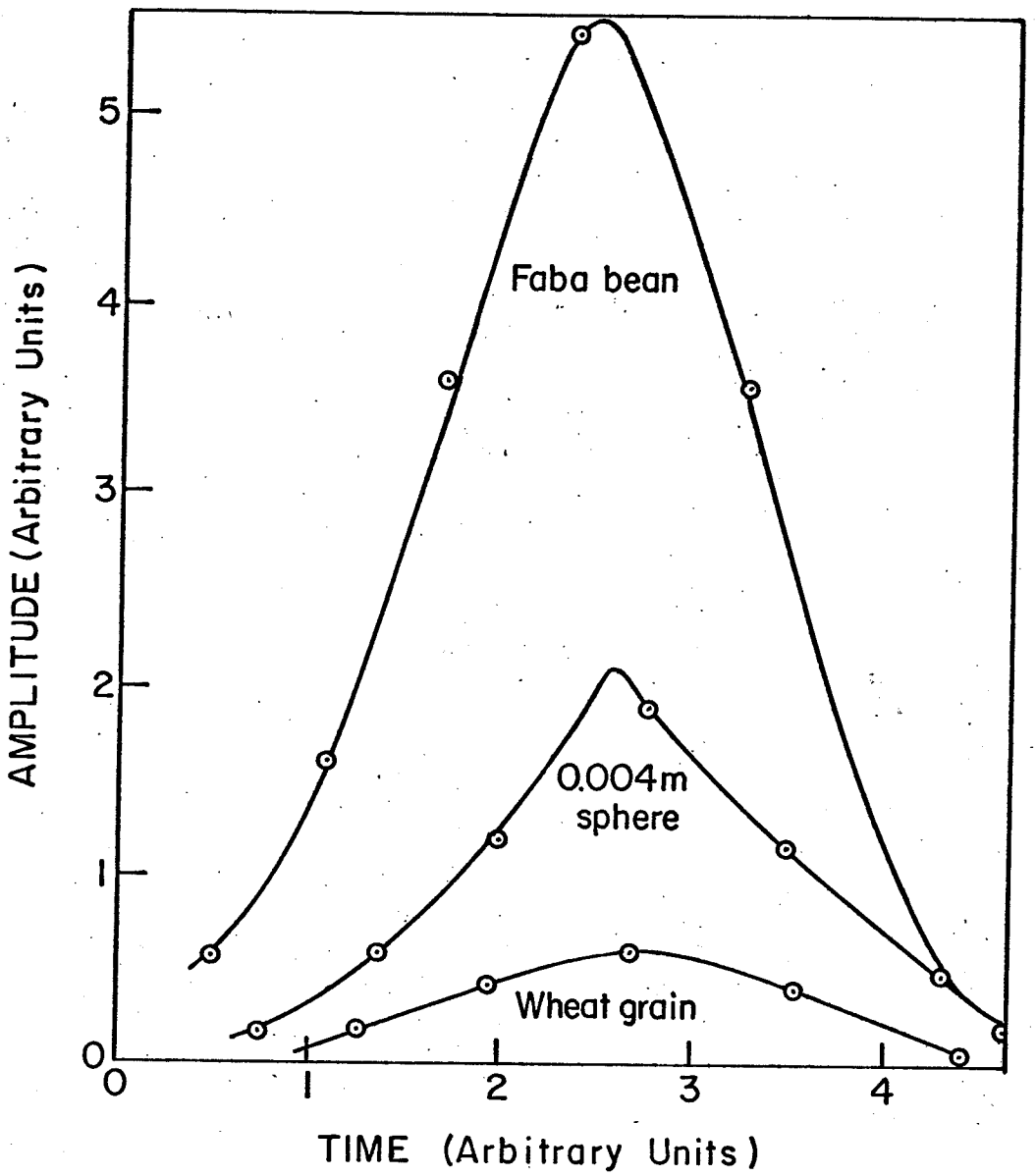

Fig. 5.7 Amplitude of the Doppler Signal as a Function of Time for Different Particles in the Free Space Configuration

$$\sigma = \left(\frac{E}{E_o}\right)^2 \sigma_o \qquad (5.8)$$

where σ is the RCS of the target of interest and σ_o is the RCS of a 0.004 m metal sphere. Furthermore, σ_o was calculated from Eq. (3.10) and was equal to 4.1×10^{-6} m^2.

Table 5.4

The RCS of Dielectric Particles Measured at Different Viewing Angles

($10^{-6} m^2$)

	45°	50°	60°
Wheat*	0.50	0.53	0.62
Wheat**	0.37	0.32	0.37
Wheat†	0.57	0.61	1.025
Rapeseed	0.024	--	0.028
Faba bean	24.6	29.6	30.1

* The main axis of the seed was parallel to the plane of polarization and the crease of the seed faced towards the ribbon

** The main axis of the seed was perpendicular to the plane of polarization and the crease of the seed faced towards the ribbon

† The main axis of the seed was parallel to the plane of polarization and the crease of the seed faced up

It is clear from Table 5.4 that the RCS is strongly dependent upon the viewing aspect, and the size and shape of the particle.

5.2 Single Particles in the Waveguide Configuration

5.2.1 Amplitude and Frequency Variations

Fig. 5.8 shows typical recordings of signals resulting from scattering by single particles moving in the rectangular waveguide. In this configuration, the target is seen by the radar at a constant viewing angle. Losses in the rectangular waveguides are negligible as compared to free space losses. For example, the attenuation in the WR-90 waveguide (used in the reported experiments) amounts to 0.12 dB/m. Therefore, the amplitude of the reflected wave should be constant and the Doppler signal should, normally, have a single discrete frequency. The amplitudes and frequencies of the Doppler signal obtained experimentally varied as the target moved across the waveguide mount. This effect is probably due to the existence of complex fields between the rectangular and cut-off circular waveguides. It should be pointed out that the scattered signal was detected up to ± 0.025 m beyond the rectangular waveguide.

The amplitudes and frequencies of the Doppler signals are plotted in Fig. 5.9 as a function of the position of the targets in the waveguide. The change in the amplitude of the Doppler signal is caused by the Doppler effect, which affects not only the frequency of the reflected signal but also its amplitude (Minervin, 1970). This effect is due to the change in phase shift of the reflected wave.

5.2.2 Velocity versus Doppler Frequency

The velocity of a particle moving through the waveguide section can be calculated by multiplying the right side of Eq. (3.2) by the ratio of the waveguide to the free space wavelength. The velocities of particles in the waveguide configuration were calculated from the relation

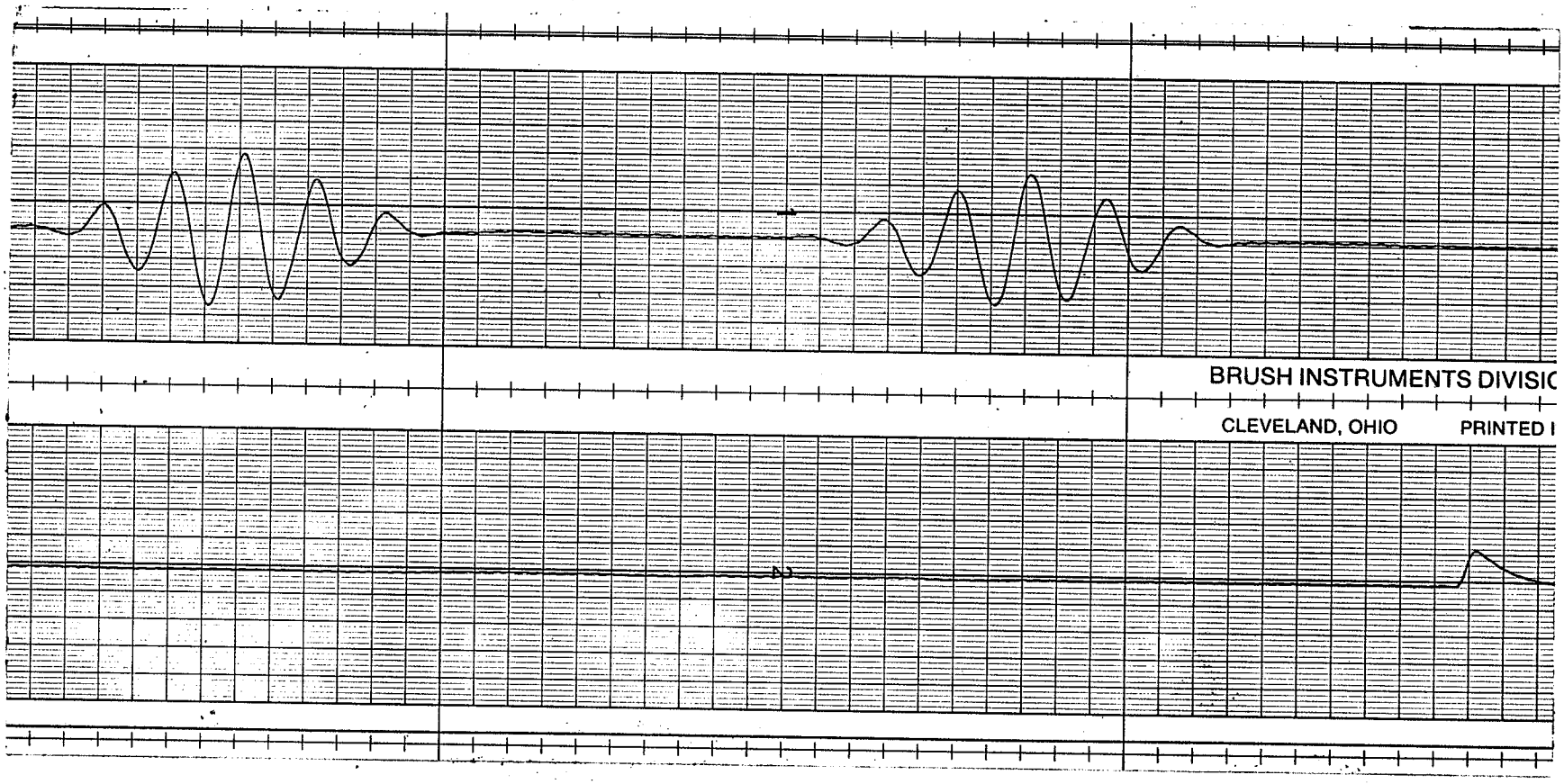

Fig. 5.8 Typical Recordings of the Doppler Signals for Single Particles in the Waveguide Configuration

[Channel 1: Signals from the Doppler radar Channel 2: Pulses from the photoresistor
Chart speed = 0.125 m/s Sensitivity of the recorded = 100 mV/div Gain of the amplifier = 200]

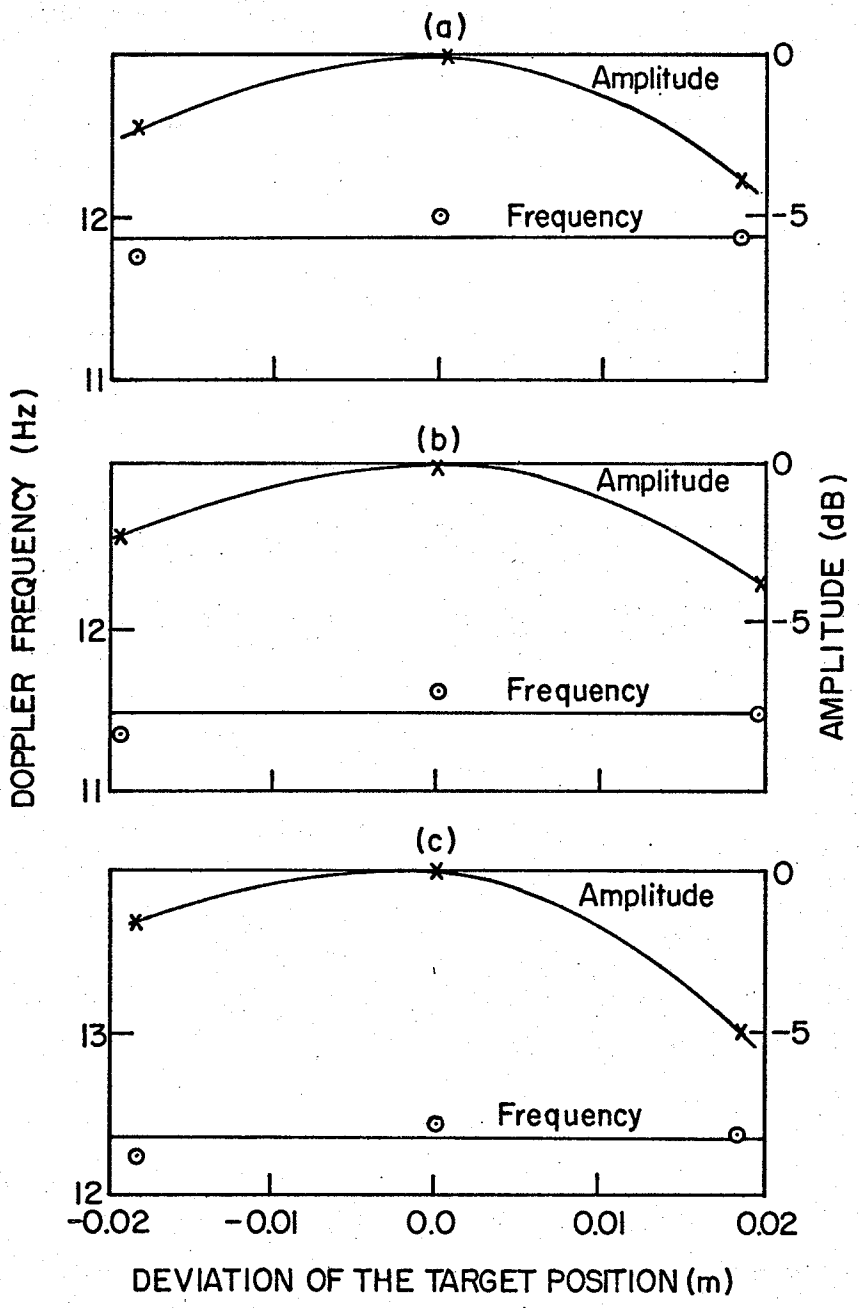

Fig. 5.9 Amplitude and Frequency of the Doppler Signal as a Function of the Target Position in the Waveguide Configuration

a) Wheat -- the Major Axis of the Seed Parallel to the Plane of Polarization

b) Wheat -- the Major Axis of the Seed Perpendicular to the Plane of Polarization

c) 0.0032 m Metal Sphere

$$v_g = k \frac{c}{2f_o} f_d/\cos\theta_g \qquad (5.9)$$

where v_g is the velocity of the particle in m/s, c is the velocity of propagation in m/s, f_o is the frequency of transmission in Hz, f_d is the Doppler frequency in Hz, and θ_g is the angle of intersection of the circular tube with the waveguide section.

In the reported experiments, θ_g was equal to 10.5° and k was equal to 1.28.

In table 5.5, the velocities indicated by the Doppler radar are compared with the velocities measured from photoresistor pulses. For most of the observations, the difference between the two velocities was not more than 2%.

5.2.3 RCS of Dielectric Particles

In the waveguide configuration, a 0.0032 m metal sphere was used as a reference to calculate the RCS of dielectric particles. The values of the RCS, listed in Table 5.6, were calculated from the relation

$$\sigma_g = \left(\frac{E}{E_o}\right)^2 \sigma_{g_o} \qquad (5.10)$$

where, σ_g is the RCS of the target of interest and σ_{g_o} is the RCS of the sphere used as a reference.

In the reported experiments, σ_{g_o} was calculated by substituting λ_g, instead of λ, in Eq. (3.10) and its value was equal to 4.17×10^{-7} m^2.

Table 5.5

Comparison between the Velocities Indicated by the Doppler Radar and Those Measured from the Photoresistor Pulses in the Waveguide Configuration

	Doppler frequency (Hz)	Velocity indicated by the radar (m/s)	Velocity calculated from the Photoresistor (m/s)	Difference %
Wheat*	11.9	0.221	0.218	-1.4
Wheat**	11.7	0.218	0.223	0.99
Metal ball 0.0032 m	12.3	0.228	0.2285	0.00
Rapeseed	12.3	0.228	0.225	-1.30
Wheat*	24.9	0.452	0.459	-0.65
Wheat**	24.5	0.455	0.459	0.87
Metal ball 0.004	24.3	0.451	0.459	1.74
0.0032	24.2	0.449	0.464	3.20
Rapeseed	24.5	0.455	0.466	2.36

* The major axis of the seed was parallel to the plane of polarization

** The major axis of the seed was perpendicular to the plane of polarization

Table 5.6

The RCS of Dielectric Particles in the Waveguide Configuration (10^{6} m^2)

	σ_g/σ_{g_o}	$\sigma_g \times \sigma 10^6$ m^2
Wheat the major axis of the seed parallel to the plane of polarization	0.334	0.14
the major axis of the seed perpendicular to the plane of polarization	0.246	0.10
Rapeseed	0.013	0.005

5.3 Continuous Flow Experiments

5.3.1 Multiple Scattering

The continuous flow of particulate solids involves a problem of multiple scattering. The Doppler signal results from contributions of signals scattered by a large number of particles.

Let us consider a relatively simple case of two independent isotropic scattering particles, illuminated simultaneously by the radar. The particles are assumed to have equal radar cross-sections. It is further assumed that both the particles are moving at the same velocity.

The voltages at the output of the radar receiver, resulting from scattering by the individual particles are given by

$$V_1 = K_2 \sin (\omega_d t + \phi_1)$$

$$V_2 = K_2 \sin (\omega_d t + \phi_2)$$

Where K_2 is a constant which includes the parameters involved in the

radar equation [Eq. (3.6)], ϕ_1 and ϕ_2 are phases of the individual echo signals, and ω_d is the angular Doppler frequency in radians.

V_1 and V_2 add vectorially so that the resultant voltage is

$$V_r = K_2 \sin(\omega_d t + \phi_1) + K_2 \sin(\omega_d t + \phi_2)$$

which may be written as

$$V_r = 2K_2 \sin(\omega_d t + \frac{\phi_1 + \phi_2}{2}) \cdot \cos \frac{\phi_1 - \phi_2}{2} \qquad (5.11)$$

Depending upon the relative values of ϕ_1 and ϕ_2, the total voltage can vary from zero to a maximum of two times the value corresponding to a single particle.

The actual case of bulk flow of granular materials is much more complicated than the simple two-scatterer case. There are several scattering particles located within the radar viewing cell. Each scattering particle has, in general, different scattering properties. Also, interactions between the scatterers affect the resultant signal. Fluctuations of the RCS with the viewing aspect add to the complexity of the problem. Furthermore, particles move neither in one direction nor at the same velocity. Random movements of particles, along with the factors discussed above, result in a complex waveform of the Doppler signal. Figs. 5.10 and 5.11 show typical recordings of the Doppler signals from bulk flow of wheat and rapeseeds, respectively. The signals are composed of bunches.

5.3.2 Averaging Technique

The discussion in the previous section leads to the conclusion that the instantaneous signal contains little practical information about the 'average' flow rate of granular materials. However, the long-time average of the instantaneous Doppler frequencies was found to be

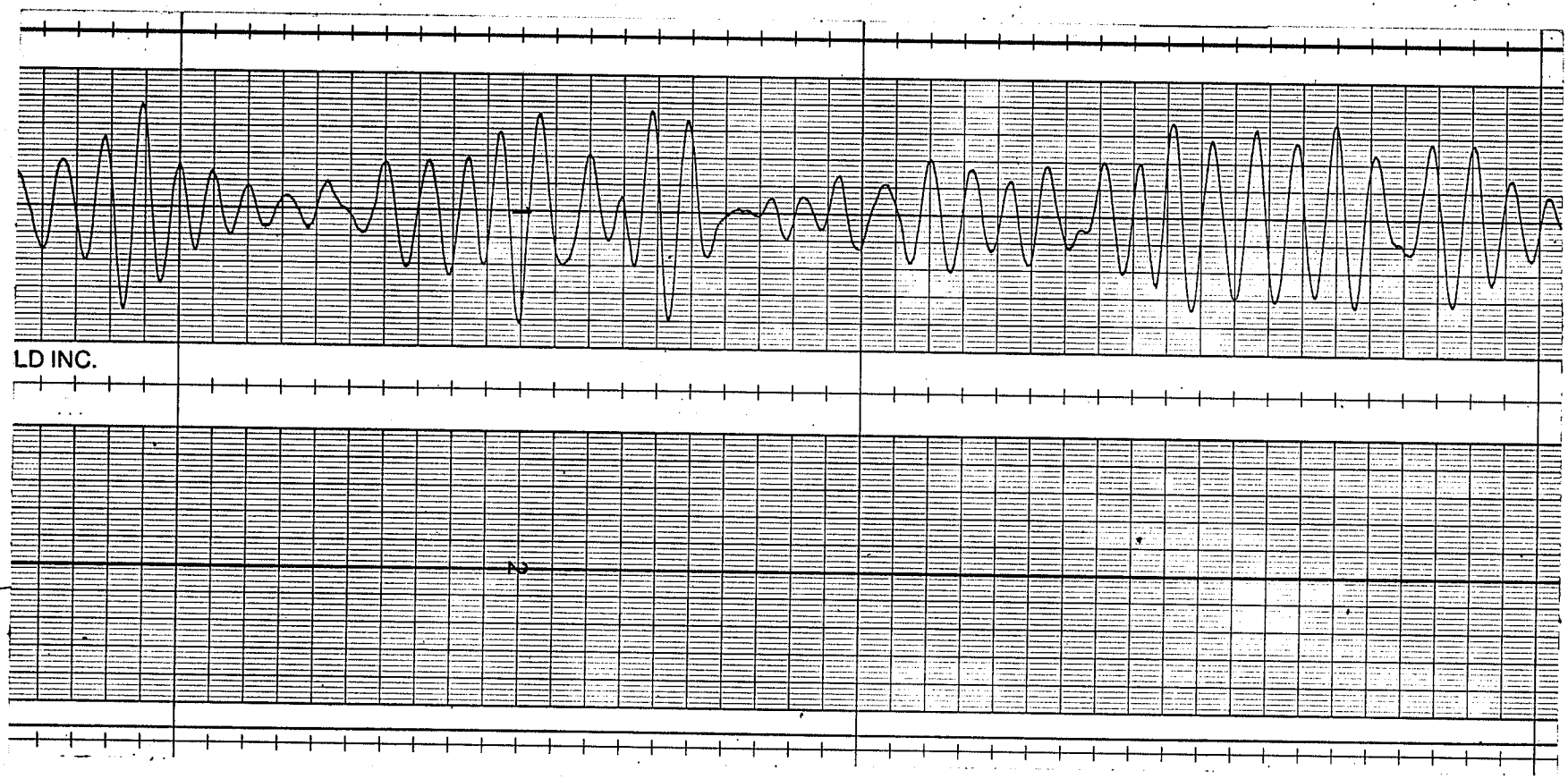

Fig. 5.10 Typical Recordings of the Doppler Signal for Bulk Flow of Wheat in the Monostatic Configuration

[Flow rate = 0.258 kg/s Viewing angle = 45° Chart speed = 0.025 m/s Sensitivity of the recorder = 50 mV/div Gain of the amplifier = 1000 V/V]

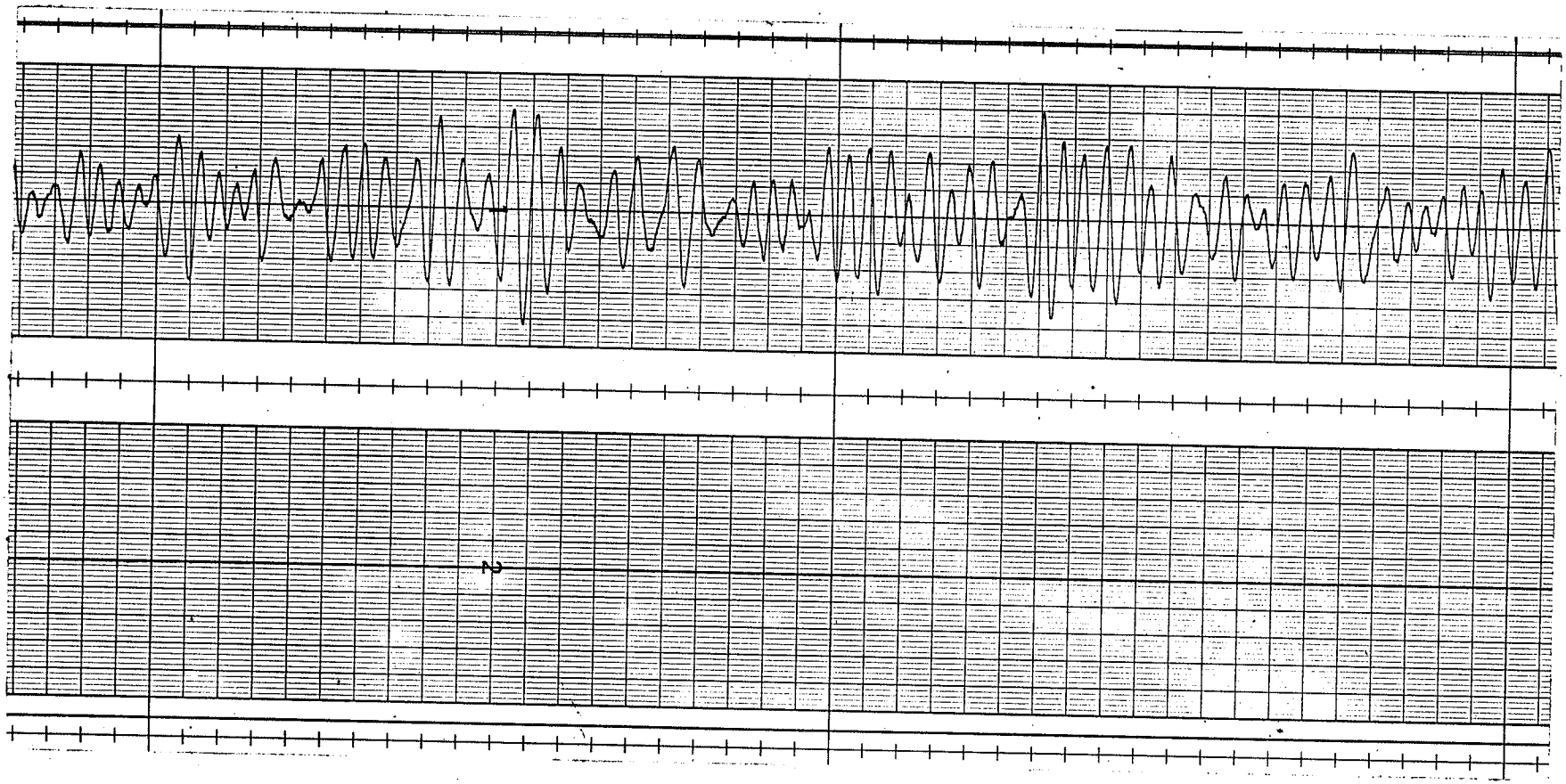

Fig. 5.11 Typical Recordings of the Doppler Signal for Bulk Flow of Rapeseeds in the Monostatic Configuration

[Flow rate = 0.448 kg/s Viewing angle = 45° Chart speed = 0.025 m/s Sensitivity of the recorder = 20 mV/div Gain of the amplifier = 1000 V/V]

proportional to the average bulk velocity. Marshal and Hitschfield (1953) have demonstrated the necessity of averaging the instantaneous signals scattered by meteorological particles in order to extract the desired information. The same averaging concept was used by Arts and Roevros (1971) to measure blood flow rates by ultrasonic means.

5.3.3. Average Bulk Flow Rate

The bulk flow of particulate solids is characterized by semi-random motions of individual particles. However, the average Doppler frequency was found to correspond to the average bulk velocity.

Using Eq. (5.1), the instantaneous Doppler frequency can be written as

$$f_{d_i} = \frac{2fo}{c} \; v_i \cos\theta_i$$

If the volume under consideration contains N particles, the average Doppler frequency is given by

$$f_{d_{av}} = \frac{1}{N} \sum_{i=1}^{N} f_{d_i}$$

$$= \frac{1}{N} \sum_{i=1}^{N} \frac{2fo}{c} \; v_i \cos\theta_i$$

$$= \frac{2fo}{c} \frac{1}{N} \sum_{i=1}^{N} v_i \cos\theta_i$$

Substituting $\bar{v} \cos\theta_o$ for $\frac{1}{N} \sum_{i=1}^{N} v_i \cos\theta_i$

$$f_{d_{av}} = \frac{2fo}{c} \; \bar{v} \cos\theta_o \qquad (5.12)$$

or

$$\bar{v} = \frac{c}{2fo} \; f_{d_{av}} \; / \cos\theta_o \qquad (5.13)$$

Where, $\bar{v}$ is the average bulk velocity in m/s, θ_o is the axial viewing angle in degrees, $f_{d_{av}}$ is the average Doppler frequency in Hz, c is the velocity of propagation in m/s and f_o is the frequency of transmission in Hz.

For a cross-sectional area A and bulk density D, the average bulk flow rate is given by

$$\bar{Q} = A \times D \times \bar{v}$$

substituting the value of $\bar{v}$ from Eq. (5.13)

$$\bar{Q} = AD \frac{c}{2fo} f_{d_{av}} / \cos\theta_o \qquad (5.14)$$

where, $\bar{Q}$ is the average mass flow rate in kg/s, A is the cross-sectional area of the flow field in m^2, D is the bulk density of the material in kg/m^3 and other symbols have the same meanings as in Eq. (5.13).

5.3.4 Integration Time

If the output of a device measuring instantaneous frequencies is averaged over a time period T, the resultant average frequency will have a standard deviation of

$$s_{f_{av}} = \frac{s_{f_i}}{\sqrt{N}}$$

where $N = \frac{2f_o}{c} \bar{v} T \cos\theta_o$

Therefore,

$$s_{f_{av}} = \frac{s_{f_i}}{\sqrt{\frac{2f_o}{c} \cos\theta_o} \sqrt{\bar{v} T}} \qquad (5.15)$$

where, $s_{f_{av}}$ is the standard deviation of the average frequency, s_{f_i} is

the standard deviation of the instantaneous frequency, $\bar{v}$ is the average velocity in m/s, T is the integration time in s, θ_o is the axial viewing angle in degrees, c is the velocity of propagation in m/s, and f_o is the frequency of transmission in Hz.

Eq. (5.15) indicates that at a constant average bulk velocity, the Doppler signal fluctuations can be decreased by increasing the integration time. Furthermore, the output signal-to-noise ratio increases with increasing integration time (Kobayashi et al., 1974) which improves the accruacy of frequency measurements [Eq. (5.5)].

An integration time of 5 seconds was found appropriate for flow rates encountered in the reported experiments. A shorter integration time was needed at high bulk velocities. However, for the sake of comparison, the same integration time was used throughout the experiments to account for non-uniformaties of flow rates.

5.3.5 Optimum Distance and Viewing Angle

The viewing angle of 45° was found most suitable for the application of the Doppler radar as a flow monitor, because:

1. Experimental uncertainties increase for viewing angles larger than 45° (Section 5.1.5), while the dielectric effects become dominant at smaller viewing angles (Section 5.3.7).
2. At smaller viewing angles the antenna beam intersects a relatively long section of the flow pipe. This results in increased fluctuations in the Doppler signal due to the variable vertical velocities. At larger viewing angles, the unwanted horizontal components of velocities become dominant. Fig. 5.12 shows the variations of the Doppler frequency (averaged over one second) as a function of time. At the viewing angle of 45°, the Doppler

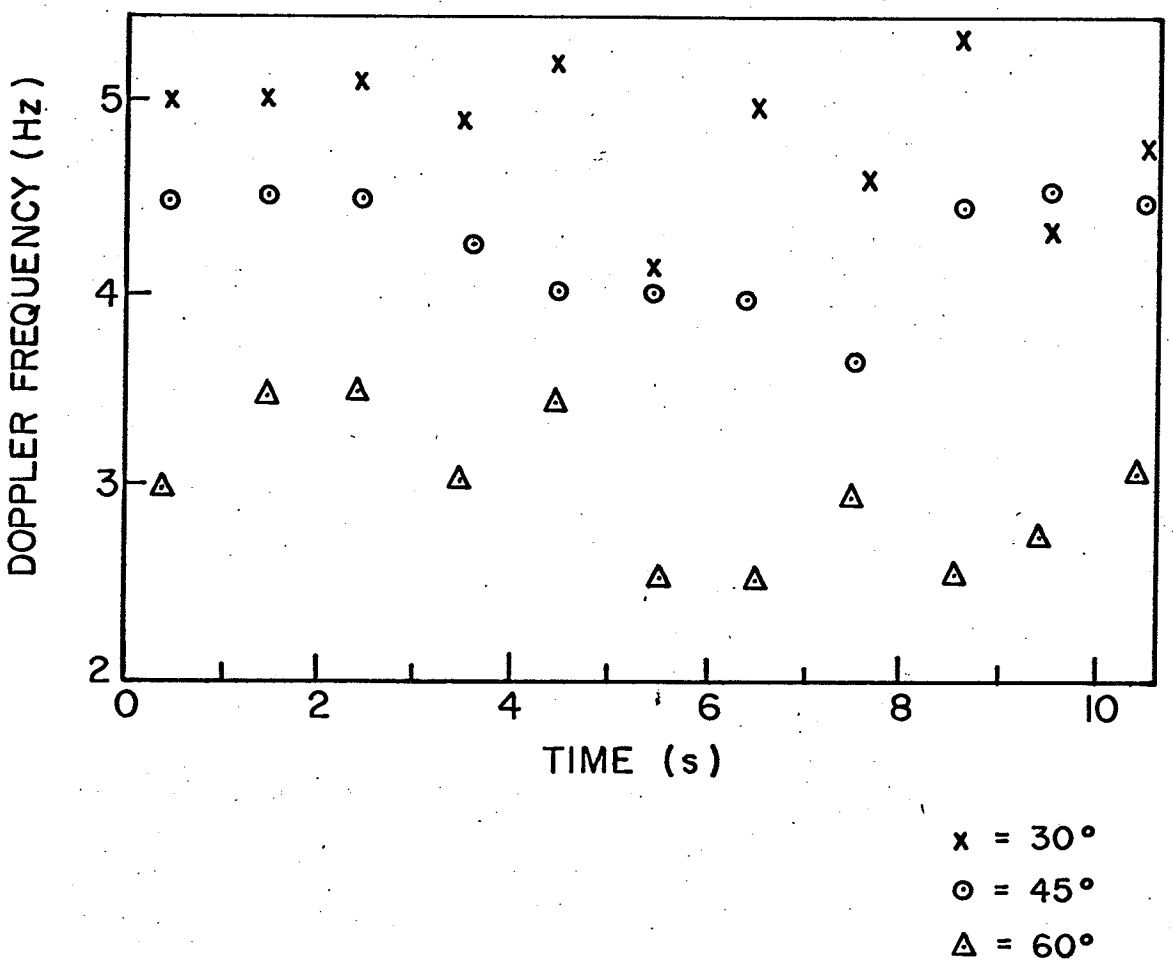

Fig. 5.12 Doppler Frequency vs Time for Continuous Flow of Wheat

signal has relatively less fluctuations.

The optimum distance between the antenna and the axis of the pipe was found to lie between W^2/λ and $2W^2/\lambda$. Here, W is the width of the antenna aperture which controls the radiation pattern in the plane of interest. Similar results have been reported by Heald et al. (1965) for plasma diagnostic with microwaves. At distances smaller than W^2/λ, the induction field effects cause large amplitude variations; while at distances larger than $2W^2/\lambda$, the probability of interference caused by spurious reflected signals becomes very high.

5.3.6 Waveguide Configuration

In the waveguide configuration, the experiments were performed with continuous flow of rapeseeds. Typical recordings of the Doppler signal are shown in Fig. 5.13. Also in this configuration, the signal is composed of bunches due to random motions of particles. Nevertheless, the flow indicated by the radar was 0.0069 kg/s as compared to 0.007 kg/s measured by the direct weighing technique. The flow rate, indicated by the radar, was calculated by mutliplying the right hand side of Eq. (5.14) with k, i.e. the ratio of the waveguide to the free space wavelength.

5.3.7 Monostatic Configuration

In Fig. 5.14, the mass flow rate, measured by the direct weighing technique, has been plotted versus average Doppler frequency. The Doppler frequency was averaged over the period of 5 seconds; the viewing angle was 45°, and the distance between the antenna and wall of the pipe was 0.1 m.

Assuming constant values of the cross-sectional area A and the bulk density D, Eq. (5.14) may be written as

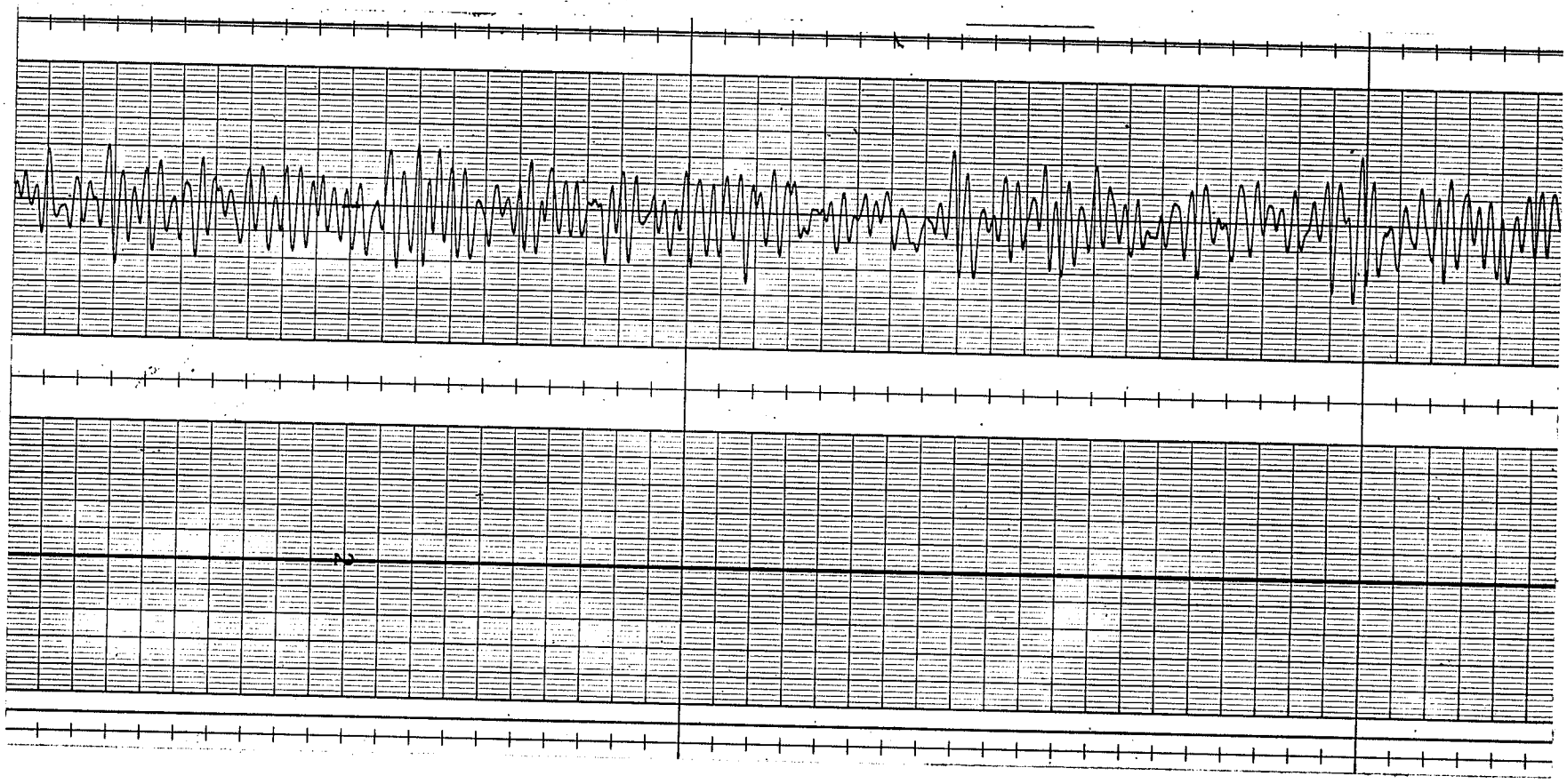

Fig. 5.13 Typical Recordings of the Doppler Signal for Continuous Flow of Rapeseeds in the Waveguide Configuration

[Flow rate = 0.007 kg/s Chart speed = 0.025 m/s Sensitivity of the recorder = 100 mV/div
Gain of the amplifier = 100 V/V]

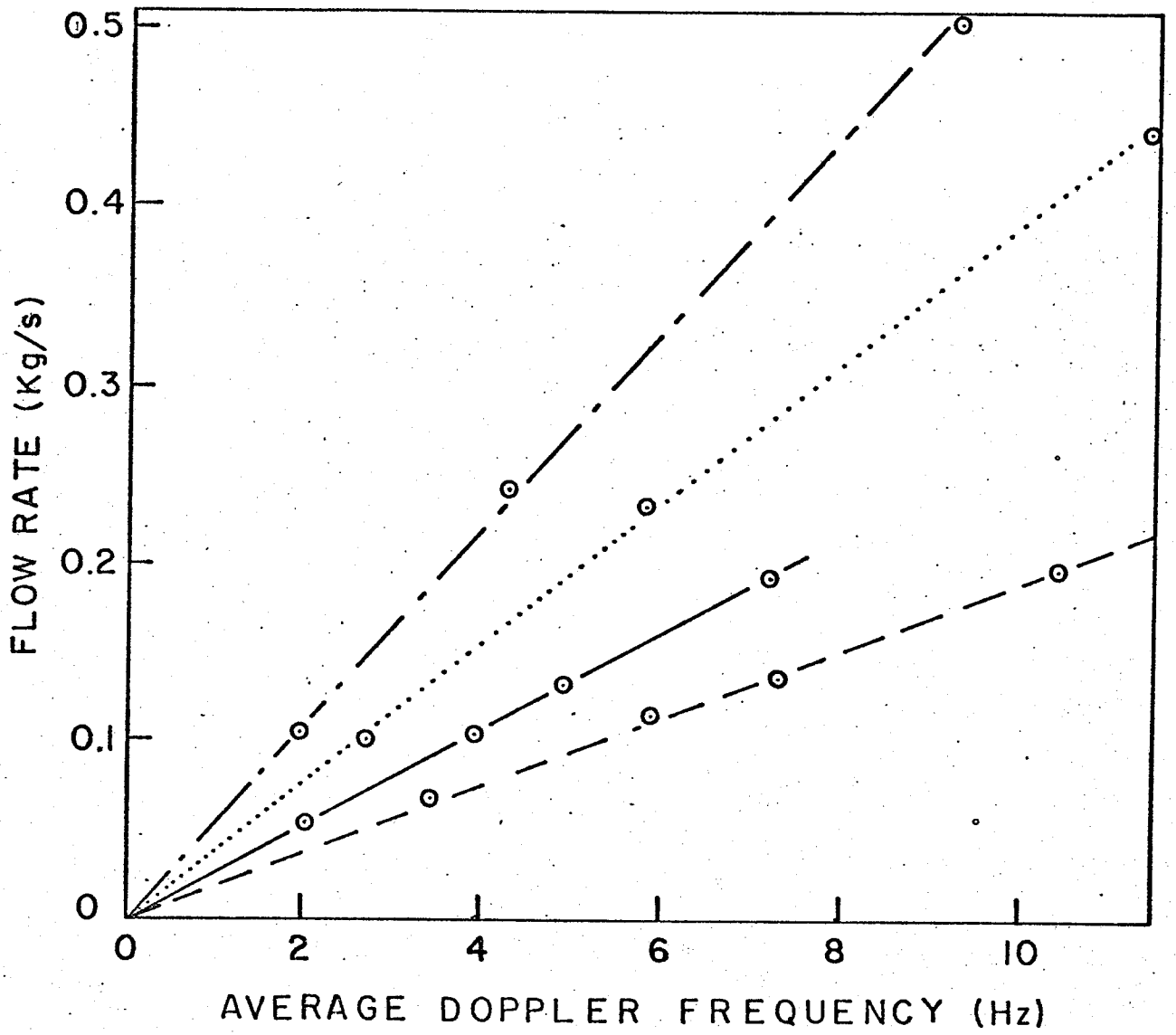

Fig. 5.14 Average Doppler Frequency vs Mass Flow Rate in the Monostatic Configuration

[The lines through the experimental points are the best fitting straight lines from the linear least square fit.

——— Wheat in 0.044 m pipe: $\overline{Q} = 0.027\ f_{d_{av}}$

——·—— Wheat in 0.0635 m pipe: $\overline{Q} = 0.054\ f_{d_{av}}$

– – – – Rapeseeds in 0.044 m pipe: $\overline{Q} = 0.02\ f_{d_{av}}$

····· Rapeseeds in 0.0635 m pipe: $\overline{Q} = 0.04\ f_{d_{av}}$]

$$\bar{Q} = Kf_{d_{av}} \tag{5.16}$$

where $$K = AD \frac{c}{2fo}/\cos\theta_o \tag{5.17}$$

Table 5.7 shows the experimental and theoretical values of K. The theoretical values of K were calculated from Eq. (5.17). The value of bulk density was 780 kg/m^3 for wheat grain and 610 kg/m^3 for rapeseed.

Table 5.7

Experimental and Theoretical values of K

	Pipe size (ID) (m)	K	
		Experimental	Theoretical
Wheat grain	0.044	0.027	0.024
	0.0635	0.054	0.05
Rapeseeds	0.044	0.02	0.019
	0.0635	0.04	0.039

The experimental values of K in Table 5.7 differ slightly from the theoretical values. This difference is caused mainly by the dielectric effects of the medium and the experimental errors in estimating the values of the bulk density and the cross-sectional area of the flow field.

Effects of the Dielectric Medium: A column of granular materials in a pipe constitutes a dielectric medium. Therefore, when the Doppler radar is used as a flow monitor, the propagation of the waves takes place partially in air and partially in the dielectric medium. For simplicity, let us assume that the Doppler frequency is changed by a factor 'a' due to these effects, so that, eq. (3.1) may be written as

$$f_d = a \cdot \frac{2f_o}{c} v \cos\theta_o \qquad (5.18)$$

Let us further assume that a single particle is moving along the axis of the pipe. If the target is in the far zone and the diameter of the column of the dielectric material is much larger than the wavelength of the incident wave, the problem may be analyzed using a plane-slab model. It is also assumed that the dielectric medium is lossless and the boundaries between the two mediums are sharp.

Referring to Fig. 5.15, the correction factor may be written as

$$a = \frac{\frac{R_o}{\lambda} + \frac{d}{2\lambda_d \cos\theta_{rf}}}{\frac{R_o}{\lambda} + \frac{d}{2\lambda \cos\theta_{id}}} \qquad (5.19)$$

where θ_{rf} is the angle of refraction in degrees, θ_{id} is the angle of incidence in degrees, Ro is the distance of propagation in free space in m, d is the diameter of the column of the dielectric medium in m, λ is the free space wavelength in m, and λ_d is the wavelength in the dielectric medium in m. Eq. (5.19) can be expanded as follows:

$$a = \frac{\frac{\cos\theta_{id}}{\cos\theta_{rf}} \times \frac{\lambda}{\lambda_d} - 1}{\frac{2Ro}{d} \cos\theta_{id} + 1} + 1$$

but $\cos\theta_{rf} = \sqrt{1-\sin^2\theta_{rf}} \simeq \sqrt{1 - \frac{\sin^2\theta_{id}}{\varepsilon'_r}}$ and $\lambda_d/\lambda \quad \sqrt{\frac{1}{\varepsilon'_r \mu}}$

where, ε'_r is the relative dielectric constant and μ'_r is the relative permittivity of the material (μ'_r is approximately equal to unity for non-magnetic materials). Substituting these values, Eq. (5.19) can be written as

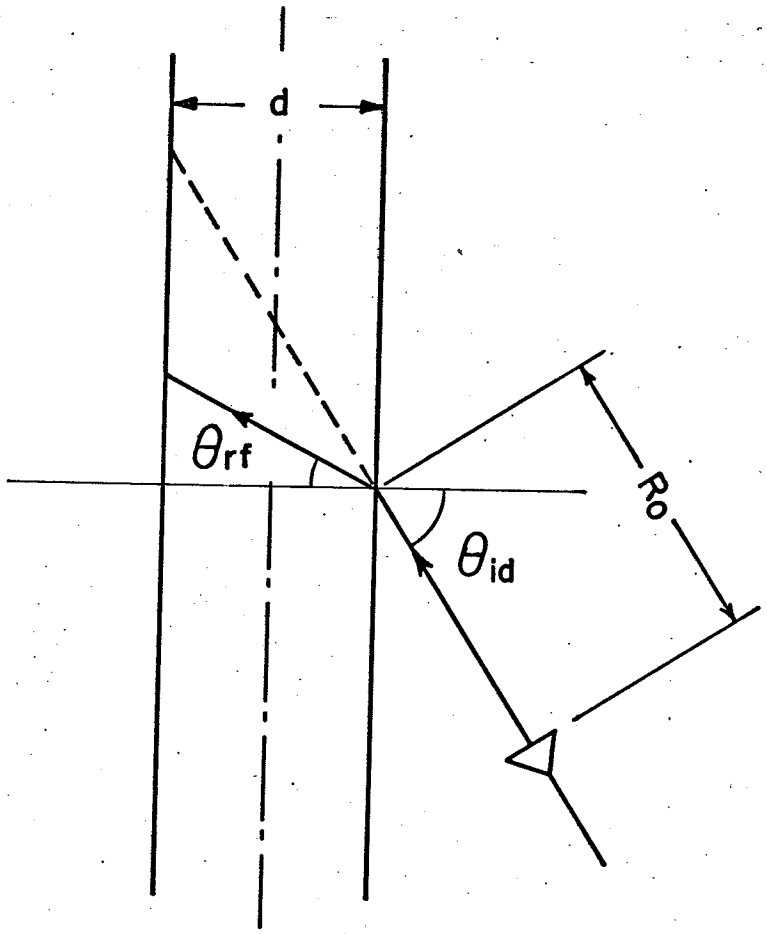

Fig. 5.15 Refraction in the Dielectric Medium -- the Plane-Slab Model

$$a = \frac{\dfrac{\cos\theta_{id}\sqrt{\varepsilon'_r}}{\sqrt{1-\sin^2\theta_{id}}} - 1}{\dfrac{2R_o}{d}\cos\theta_{id} + 1} + 1$$

which may be written as

$$a = \frac{\dfrac{\cos\theta_{id}\,\varepsilon'_r}{\sqrt{\varepsilon'_r - \sin^2\theta_{id}}} + \dfrac{2R_o}{d}\cos\theta_{id}}{\dfrac{2R_o}{d}\cos\theta_{id} + 1}$$

But $\theta_{id} = 90° - \theta_o$

Therefore,

$$a = \frac{\dfrac{\sin\theta'_o\,\varepsilon'_r}{\sqrt{\varepsilon'_r - \cos^2\theta_o}} + \dfrac{2R_o}{d}\sin\theta_o}{\dfrac{2R_o}{d}\sin\theta_o + 1} \qquad (5.20)$$

where, θ_o is the viewing angle, ε'_r is the relative dielectric constant of the bulk material under test, and other symbols have the same meaning as in Eq. (5.19)

For $R_o = 0$

$$a = \frac{\sin\theta_o\,\varepsilon'_r}{\sqrt{\varepsilon'_r - \cos^2\theta_o}} \qquad (5.21)$$

For $R_o = 0$, $\theta_o = 90°$

$$a = \sqrt{\varepsilon'_r} \qquad (5.22)$$

Effects of the dielectric medium are far more complicated than those predicted by Eq. (5.19). The microwave beam is affected by the

presence of a large number of dielectric particles, each having a different index of refraction. Nevertheless, it can be deduced that these effects decrease with increasing viewing angle, and become negligible if R_o/d is very large.

The relationship between the average Doppler frequency and the average bulk velocity is linear. Therefore, the value of K can be easily determined experimentally.

High Bulk Velocities: High velocities were obtained by using flow control disks at the upper end of the flow pipes. Typical recordings of the Doppler signals are shown in Figs. 5.16 and 5.17. Since R_o/d is very large in this case, the dielectric effects can be neglected. Tables 5.8 and 5.9 show the comparison of experimental and theoretical values of bulk velocities. The experimental values were calculated from Eq. 5.13, while theoretical values were estimated as follows:

If the effects of frictional forces are neglected, the maximum theoretical velocity of the free flow is given by

$$v_m = \sqrt{u^2 + 2gy} \tag{5.24}$$

where, u is the initial velocity in m/s, g is the acceleration due to gravity in m/s^2, and y is the vertical distance to the point of observation in m.

The initial velocity u was estimated by

$$u = \frac{\bar{Q}}{A_1 D} \tag{5.25}$$

where, $\bar{Q}$ is the average mass flow rate in kg/s, D is the bulk density in kg/m^3 and A_1 is the cross-sectional area of the flow field in m^2.

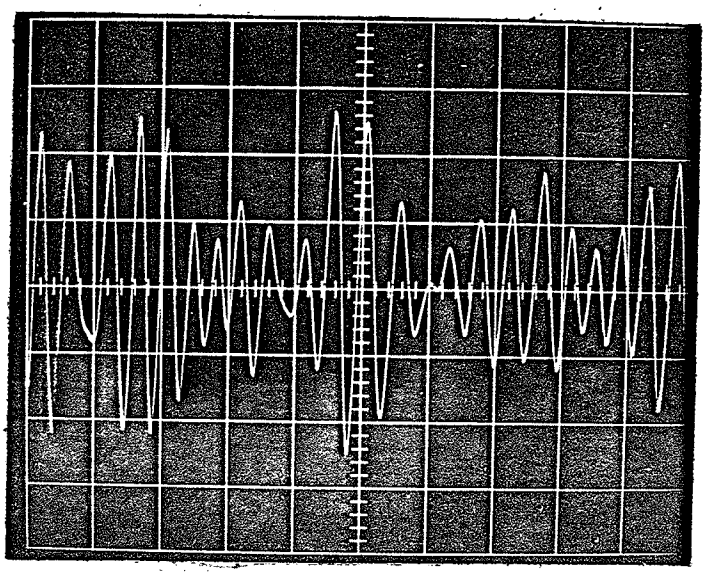

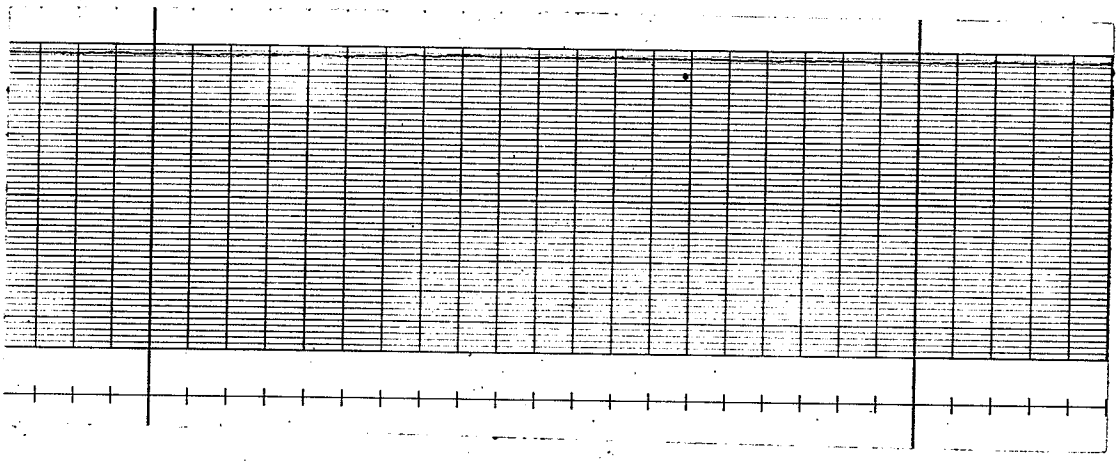

Fig. 5.16 Doppler Signals for Continuous Flow of Wheat at High Bulk Velocities in the Monostatic Configuration
[Flow rate = 0.117kg/s]

(a) Oscillogram
[Scale: Vertical = 0.2 V/div Horizontal = 20 ms/div
Gain of the amplifier = 500]

(b) Recordings from an Analog Frequency Meter
[Sensitivity of the recorder = 4.66 Hz/div.]

(c)

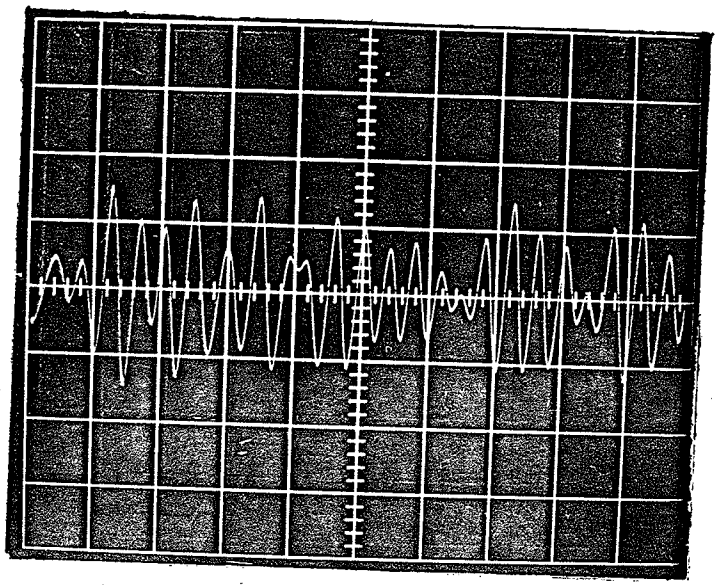

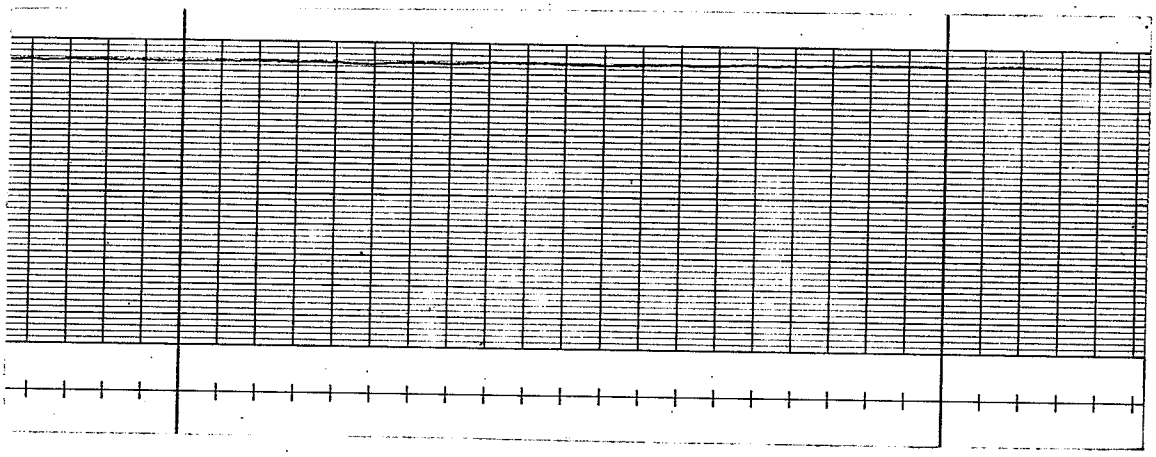

Fig. 5.17 Doppler Signals for Continuous Flow of Rapeseeds at High Bulk Velocities in the Monostatic Configuration
[Flow rate = 0.812 kg/s]

(a) Oscillogram
[Scale: Vertical = 0.2 V/div Horizontal = 20 ms/div
Tain of the amplifier = 200]

(b) Recordings from an Analog Frequency Meter
[Sensitivity of the recorder = 4.66 Hz/div.]

In the reported experiments, y was equal to 0.276 m and values of other variables were the same as stated previously for low bulk velocities.

Table 5.8

Comparison of the Experimental and Theoretical Bulk Velocities of Wheat Grain

Pipe size (m)	Flow rate (kg/s)	Theoretical velocity v_m (m/s)	Average Doppler frequency (Hz)	Velocity indicated by the Doppler radar, $\bar{v}$ (m/s)	$\bar{v}/v_m$
0.044	0.064	2.33	102.3	2.06	0.88
	0.117	2.34	104.6	2.11	0.90
	0.144	2.34	104.6	2.11	0.90
	0.186	2.34	104.6	2.11	0.90
0.0635	0.136	2.34	109.3	2.20	0.94
	0.270	2.34	110.4	2.22	0.95
	0.513	2.35	107.1	2.16	0.92
	0.959	2.36	107.1	2.16	0.92

Table 5.9

Comparison of the Experimental and Theoretical Bulk Velocities of Rapeseeds

Pipe size (m)	Flow rate (kg/s)	Theoretical velocity, $\bar{v}_m$ (m/s)	Average Doppler frequency (Hz)	Velocity indicated by the Doppler radar, $\bar{\bar{v}}$ (m/s)	$\bar{\bar{v}}/\bar{v}_m$
0.044	0.070	2.34	107.9	2.17	0.93
	0.117	2.34	105.6	2.13	0.91
	0.144	2.34	105.4	2.12	0.91
	0.180	2.35	103.1	2.08	0.89
	0.446	2.375	106.2	2.14	0.90
0.0635	0.131	2.35	107.6	2.17	0.92
	0.280	2.35	108.0	2.18	0.93
	0.490	2.36	105.5	2.13	0.90
	0.813	2.36	103.7	2.09	0.89

Tables 5.8 and 5.9 indicate that the theoretical velocities are higher than those indicated by the Doppler radar. This is because the effects of the frictional forces were neglected in estimating the theoretical values. In the larger pipe (0.0635 m), particles have relatively less chances of colliding with the pipe walls and, therefore, the effects of frictional forces are not as pronounced as in the smaller pipe (0.044m).

5.3.8 Bistatic Configuration

Experiments in the bistatic configuration were performed with the continuous flow of wheat. If both the transmitter and receiver are located at equal distances from the target and θ_r is equal to θ_t, the equations in the monostatic configuration can be applied to the bistatic configuration.

The experiments were performed with viewing angles of 45° for both the transmitter and receiver. Both the transmitter and receiver were located at distances of 0.1 m from the walls of the pipe. Typical recordings of the Doppler signals are shown in Fig. 5.18.

The flow rate, measured by the direct weighing technique, was plotted versus the average Doppler frequency in Fig. 5.19. The experimental values of K in this case are: 0.028 for the 0.044 m pipe and 0.054 for the 0.0635 m pipe. These values are approximately the same as obtained in the monostatic configuration (Table 5.7). This is understandable, since the experimental conditions in this case approximate the monostatic configuration (Section 5.3.7).

Verification of the Flow Rate Equation at Different Viewing Angles: In general, the flow rate equation in the bistatic configuration can be written as

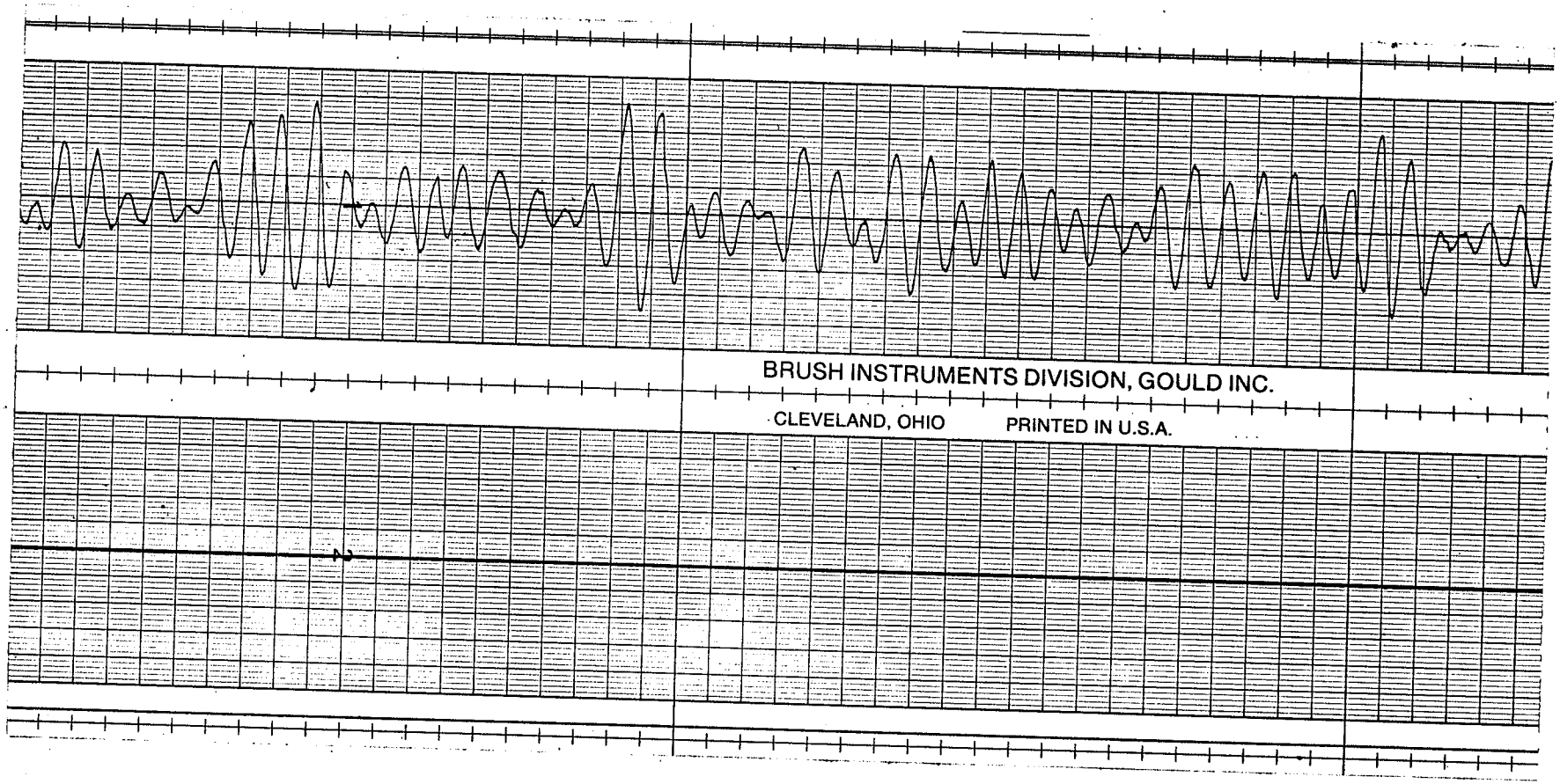

Fig. 5.18 Typical Recordings of the Doppler Signal for Continuous Flow of Wheat in the Bistatic Configuration

[Flow rate = 0.134 kg/s Chart speed = 0.025 m/s Sensitivity of the recorder = 20 mV/div
Gain of the amplifier = 1000 V/V]

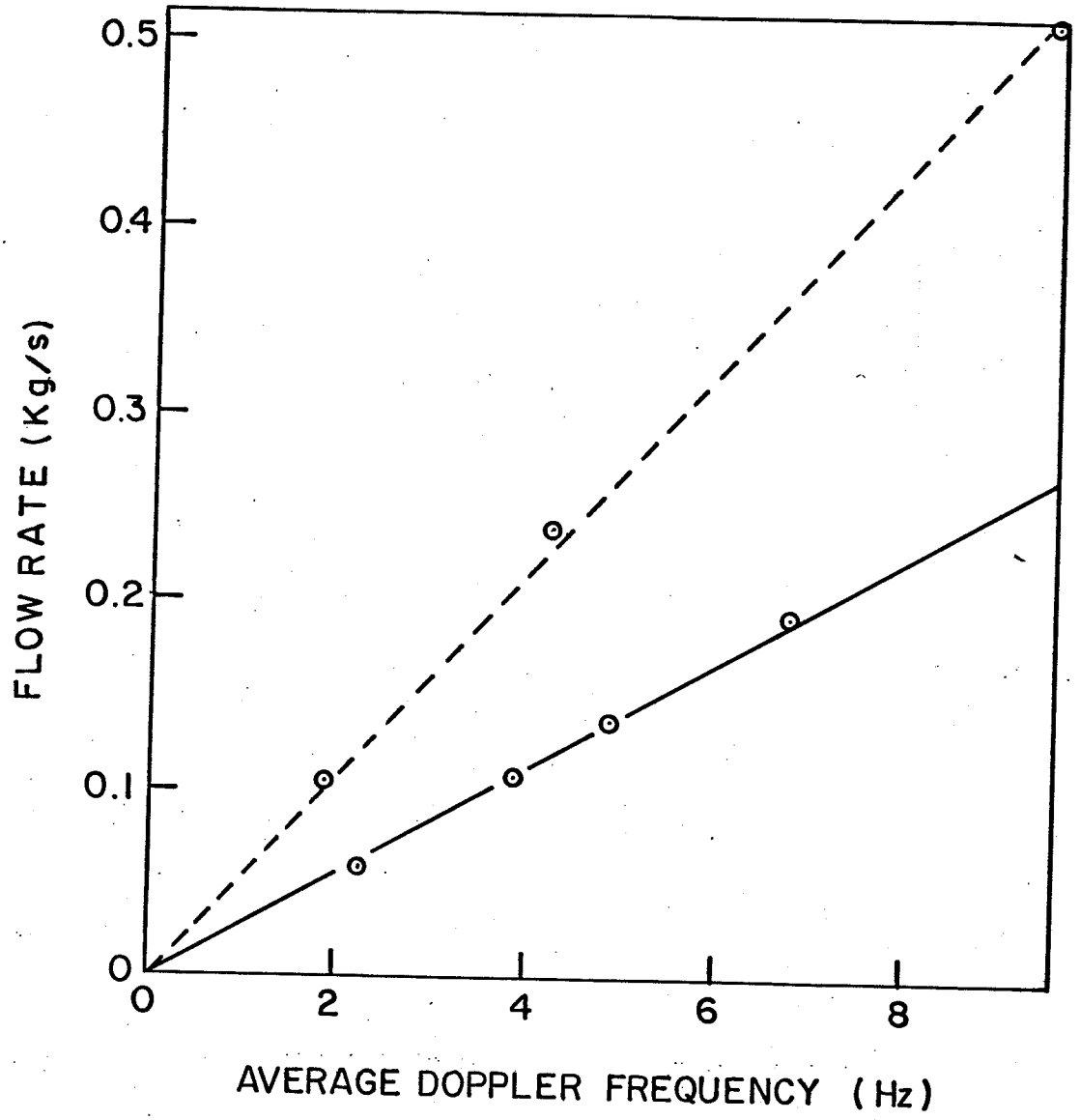

Fig. 5.19 Average Doppler Frequency vs Mass Flow Rate for Wheat in the Bistatic Configuration

[The lines through the experimental points are the best fitting straight lines from the linear least square fit.

——— 0.044 m pipe: $\overline{Q} = 0.028\ f_{d_{av}}$

– – – – – 0.0635 m pipe: $\overline{Q} = 0.054\ f_{d_{av}}$]

$$\bar{Q} = AD \frac{c}{fo} f_{d_{av}} / (\cos\theta_t + \cos\theta_r) \qquad (5.26)$$

where, $\bar{Q}$ is the average mass flow rate in kg/s, $f_{d_{av}}$ is the average Doppler frequency and other symbols have the same meaning as in Eq. (3.4).

Eq. (5.26) was verified experimentally for wheat. The viewing angle of the transmitter was maintained at 45°, while the viewing angle of the receiver was varied from 30° to 60°. The frequency of the Doppler signal obtained at viewing angles of 45° for both the transmitter and receiver was used as reference. Typical recordings of the Doppler signal are shown in Fig. 5.20.

The experimental and theoretical values of the average Doppler frequency are shown in Table 5.10. The theoretical values were calculated as follows:

For the viewing angles of 45° for both the transmitter and receiver, the average Doppler frequency can be written as

$$f_{d_{45}} = \frac{2fo}{c} \frac{\bar{Q}}{DA} \cos \pi/4$$

And for any arbitrary angle of the receiver

$$f_{d_{\theta_r}} = \frac{fo}{c} \frac{\bar{Q}}{DA} (\cos\pi/4 + \cos\theta_r)$$

so that

$$\frac{f_{d_{\theta_r}}}{f_{d_{45}}} = \frac{\cos\pi/4 + \cos\theta_r}{2\cos\pi/4}$$

Thus

$$f_{d_{\theta_r}} = f_{d_{45}} \cdot \frac{\cos\pi/4 + \cos\theta_r}{2\cos\pi/4} \qquad (5.27)$$

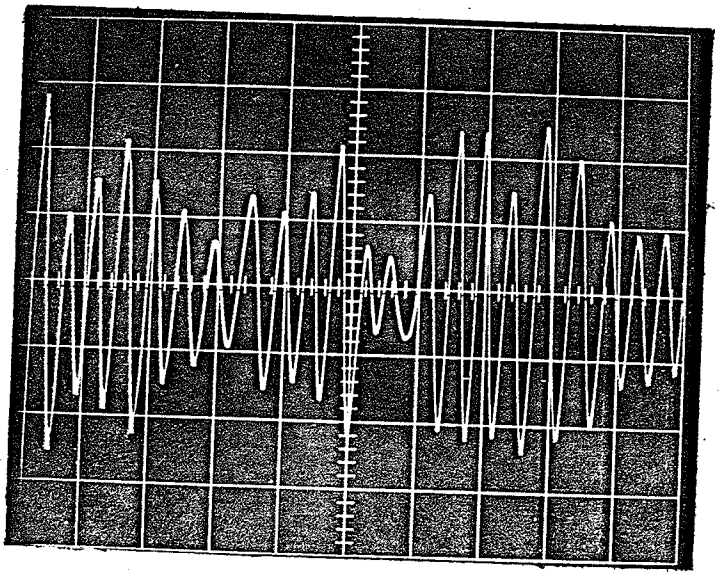

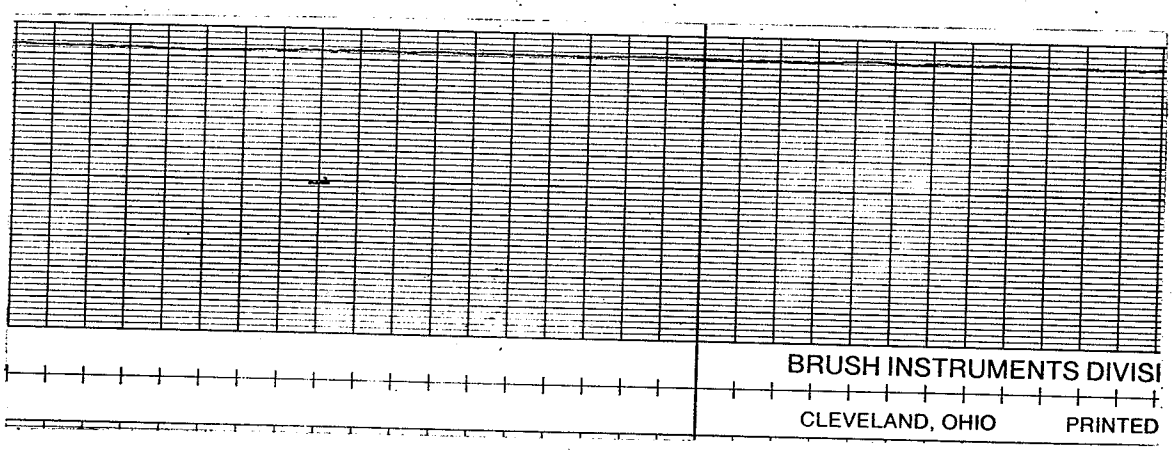

Fig. 5120 Doppler Signals for Continuous Flow of Wheat at High Bulk Velocities in the Bistatic Configuration

[Viewing angle for both the transmitter and receiver = 45°
Flow rate = 0.532 kg/s]

(a) Oscillogram
[Scale: Vertical = 0.1 V/div Horizontal = 20 ms/div
Gain of the amplifier = 200]

(b) Recordings from an Analog Frequency Meter
[Sensitivity of the recorder = 4.66 Hz/div]

Table 5.10

The Experimental and Theoretical Values of the Average Doppler Frequencies in the Bistatic Configuration at Different Viewing Angles of the Receiver

Receiver viewing angle (degrees)	Average Doppler frequency (Hz)	
	Experimental	Theoretical
45	101.8	
40	106.4	106.0
50	95.7	97.2
55	92.2	92.2
60	85.5	86.9

Table 5.10 indicates that the experimental values of the average Doppler frequencies are in good agreement with the theoretical values. This leads to the conclusion that the MDEF in the bistatic configuration can be applied to monitor the flow rates of particulate solids.

CHAPTER 6

CONCLUSIONS

As a result of this research, it seems possible to utilize the microwave Doppler radar to measure the average bulk velocity of particulate solids flowing in pipes. If the cross-sectional area of the flow field and material density are known, the average bulk velocity is proportional to the mass flow rate. Thus, the MDEF provides a contactless means of monitoring the flow rate of particulate solids.

The frequency of the Doppler signal from single scattering particles was found to be spread over a finite bandwidth. The mean frequency of the Doppler spectrum gives the accurate value of the velocity for a given viewing angle.

The bulk flow of particulate solids involves a problem of multiple scattering. Semi-random movements of particles in the flow field result in a complex waveform of the Doppler signal. The signal had to be averaged over a certain period of time in order to extract the desired information. An integration time of 5 seconds was found sufficient to measure the average Doppler frequency for uniform bulk velocity of the material.

The effect of refraction at the boundary between air and material has been analysed. The average Doppler frequency is a linear function of the average bulk velocity and, therefore, the proportionality constant between the two can be easily determined experimentally for a given system.

Although both the monostatic and bistatic configurations of the MDEF are possible, the monostatic configuration is more economical and easier to install and operate in industrial conditions.

In the monostatic configuration, a viewing angle of 45° was found optimum, while the recommended distance between the antenna aperture and flow field lies between W^2/λ and $2W^2/\lambda$.

The MDEF measures the average flow rate without obstructing or disturbing the system conveying the test material. Low cost, simplicity and very high reliability of modern solid state Doppler transceivers make their application as industrial flowmeters very attractive from both technical and economic point of view.

REFERENCES

[1] Arts, M.G.J. and J.M.J.G. Roevros. 1972. On the instantaneous measurement of blood flow by ultrasonic means. Med. and Biological Engineering. 10:23-34.

[2] Barlow, E.J. 1949. Doppler radar. Proc. IRE. 37:340-355.

[3] Beck, M.S., J. Drane, A. Plaskowski, and N. Wainwright. 1968. New method of measuring mass flow of powder in pneumatic conveyor using on-line computer. Instn. Elec. Engrs, London, England, Conference Publ. n43: 133-147.

[4] Beck, M.S. and N. Wainwright. 1969. Current industrial methods for solid flow detection and measurement. Powder Technol., 24:189-197.

[5] Berger, F.B. 1957. The nature of Doppler velocity measurement. IRE Trans. ANE 4:103-112.

[6] Bousser, J.E. 1904. Governor for grain feed. U.S. patent 764,705.

[7] Brown, S.G., T.M. Bates and J.E. Wilhelm. 1962. Flame monitoring and combustion stability. ASME. Paper No. 62-WA-186.

[8] Carlson, H.M., P.M. Frazier and R.B. Engdahl. 1948. Meter for flowing mixtures of air and pulverised coal. ASME. Trans. 10: 65-73.

[9] Chugh, R.K., S.S. Stuchly, and M.A. Rzepecka. 1973. Dielectric properties of wheat at microwave frequencies. Trans. of ASAE, 16(5): 906-909,913.

[10] Considine, D.M. and S.D. Ross. 1964. Handbook of applied instrumentation. McGraw Hill, New York.

[11] Cotton, K.C., ed. 1966. Flow measurement symposium. ASME, New York.

[12] Craven, G.F. 1964. Automatic weighing and batching of bulk solids. Chem. and Process Eng. 45: 125-128.

[13] Crispin Jr., J.W. and A.L. Maffett. 1965. Radar cross-section estimation for simple shapes. IEEE Proc. 53(8): 833-848.

[14] Crispin, J.W. and K.M. Siegel, ed. 1968. Methods of radar cross-section analysis. Academic Press, New York and London.

[15] Dean, S.K. 1955. Flowmeter for granular material. Engineering 179(4654): 430-431.

[16] DISA. 1973. Bibliography of laser Doppler anemometry literature. DISA Electronics A/S, DK-2730, Herlev, Denmark.

[17] Edwards, R.V. et al. 1971. Spectral analysis of signal from laser Doppler flowmeter. J. Appl. Phys. 42(2): 837-850.

[18] Ehrman, L. 1964. Analysis of a zero-crossing frequency discriminator with random inputs. IEEE Trans. ANE 12: 113-119.

[19] Ellerbruch, D.A. 1970. Microwave methods for cryogenic liquid and slush instrumentation. IEEE Trans. IM 19(4): 412-416.

[20] Farbar, L. 1952. The venturi as a meter for gas - solids mixtures. ASME Paper No. 52-A-31.

[21] Henderson, J.M. 1966. A mass flow meter for granular material. ISA Trans. 5: 78-83.

[22] Hannir, J. 1970. Radascan flow/no flow detector. Measurement and Control 3(12): 356.

[23] Harris, J. 1970. Interogating flow fields with radar and laser sources. Measurement and Control 3(11): 188-192.

[24] Heald, M.A. and C.B. Wharton. 1965. Plasma diagnostics with microwaves. John Wiley & Son Inc. New York.

[25] Hp. 1971. X-band Doppler radar modules. Hewlett Packard technical data, 25M1171.

[26] Keller, D.L. et al. 1971. Measuring corn kernel velocities in a pneumatic conveyor by a radio active tracer technique. ASAE. Paper No. 71-308.

[27] Kirwan, J.O. and L.E. Demler. 1955. Continuous weighing and feeding. Instr. and Automation. 28: 98-101.

[28] Kobayashi, M. et al. 1974. On the mean frequency measurement system using correlating detection. IEEE Trans. AES 10(3): 364-371.

[29] Lazanby, B.D. and M.A.S. Davies. 1973. Solutions to monitoring of particulate solids. Control and Instrumentation 5(1): 29-30.

[30] Marshall, J.S. and W. Hitschfeld. 1953. The interpretation of fluctuating echo from randomly distributed scatterers. Canadian Journal of Physics. 31: 962.

[31] Merchen, G.G. 1929. Automatic Weighing Machine. U.S. Patent 1,728,429.

[32] Minervin, N.N. 1971. Accuracy of measurement of Doppler frequency shift. Radio Eng. Electron Phys. 16(8): 1299-1303.

[33] Nolte, C.B. 1969. Flowmeter for solid particulate materials. Proc. of the 24th Annual ISA Conf. Paper No. 69-527.

[34] Parker, R.R. 1970. A microwave Doppler flowmeter. MIT Report 2-8-141.

[35] Pawula, R.B. 1968. Analysis of an estimator of the center frequency of a power spectrum, IEEE Trans. IT 14(5): 669-676.

[36] Powley. C. 1972. In-line meter removes barrier to accurate solids flow measurement. Process Engg. (September 1972): 115-117.

[37] Skolnik, M.T. 1962. Introduction to radar system. McGraw Hill, New York.